

UNIVERSITÀ DEGLI STUDI DI PADOVA

FACOLTÀ DI SCIENZE MM. FF. NN.

Dipartimento di Geoscienze

Direttore Prof. Fabrizio Nestola

TESI DI LAUREA MAGISTRALE

IN

GEOLOGIA E GEOLOGIA TECNICA

**THE EOCENE/OLIGOCENE BOUNDARY IN THE  
LESSINI SHELF - FACIES ANALYSIS AND  
CARBONATE STABLE ISOTOPE GEOCHEMISTRY**

*Relatore: Prof. Nereo Preto*

*Correlatore: Prof.ssa Claudia Agnini*

*Laureanda: Federica Chimento*

ANNO ACCADEMICO 2019/2020

# Index

ABSTRACT .....	1
INTRODUCTION .....	2
Study area.....	3
METHODS .....	12
Sample collection .....	12
Calcareous Nannofossils.....	14
Isotopic sample preparation and analysis.....	15
RESULTS .....	19
Nannofossils.....	19
Facies of the Castelgomberto formation.....	28
Carbon and oxygen stable isotope data .....	36
Calcium carbonate content.....	43
DISCUSSION .....	45
Facies analysis .....	45
Calcareous nannofossil biostratigraphy and biochronological implications .....	46
Isotopic data interpretation .....	50
CONCLUSIONS .....	55
Acknowledgments .....	56
Bibliography.....	57
Appendix.....	61

## ABSTRACT

In this thesis, the Castelgomberto and Santa Tecla sections (Northeast of Italy) were analyzed with the aim to produce a new dataset from the Castelgomberto formation, a shallow water carbonate unit of Early Oligocene age that crops out in the Vicentinian pre-Alps, Northern Italy, and sits directly on the Eocene/Oligocene boundary. New samples of rocks, oysters, pectinids and clay have been collected.  $\delta^{13}\text{C}$  VPDB and  $\delta^{18}\text{O}$  VPDB values were measured on oyster, pectinid and rock samples while clayey samples were processed for nannofossil counting. Results from nannofossil dating confirm previous dating for the base of Castelgomberto formation, but reveal that only the first nannofossil biochronozone of the Oligocene is present, which possibly implies a sedimentary gap in the study area at the top of the formation. Isotopic data of carbon were used for a correlation with the global/reference isotopic curve.

In questa tesi vengono analizzate le sezioni di Castelgomberto e Santa Tecla (Veneto, Italia) con lo scopo di fornire nuovi dati per la formazione di Castelgomberto, un'unità carbonatica di mare basso di età Oligocene inferiore che affiora nelle prealpi vicentine, nord Italia, e che poggia direttamente sul limite Eocene/Oligocene. Sono stati raccolti nuovi campioni di roccia, ostriche, pettinidi e dei campioni argillosi. Sono stati misurati i valori di  $\delta^{13}\text{C}$  VPDB e  $\delta^{18}\text{O}$  VPDB per i campioni di ostriche, pettinidi e di roccia, mentre i campioni argillosi sono stati utilizzati per l'analisi delle associazioni a nannofossili calcarei. La biostratigrafia a nannofossili calcarei conferma i risultati già disponibili in letteratura per la base della formazione ma rivela anche che solo la prima biozona a nannofossili calcarei dell'Oligocene è presente, suggerendo quindi la presenza di un gap sedimentario nell'area di interesse al tetto della formazione di Castelgomberto. Inoltre i dati isotopici del carbonio sono stati correlati con la curva isotopica globale.

# 1. INTRODUCTION

The Earth has gone through four climate states during the Cenozoic. The study of carbon and oxygen isotopes measured on benthic foraminiferal tests has allowed to identify these climate states on the basis of their distinctive response to astronomical forcing depending on the greenhouse gas concentrations and polar ice sheet volume (Westerhold et al., 2020). This dataset also demonstrates that orbital variations affect global carbon cycle, modulate solar forcing and trigger glacial events (Pälike et al., 2006). Warmhouse and Hothouse states prevailed from the Cretaceous/Paleogene boundary (K/Pg, 66 Ma) to the Eocene-Oligocene Transition (EOT, 34 Ma Coxall and Pearson, 2007). At EOT, the Earth was in a Warmhouse state and transitioned into Coolhouse state (Westerhold et al., 2020).

The Eocene-Oligocene transition has been investigated under various aspects and it has been found that during this time several changes occurred. Geological and geochemical evidences indicate that the Antarctic ice sheet eventually formed during the EOT, 33.5-34 Million years ago (Pearson et al., 2009). The drawdown of atmospheric  $p\text{CO}_{2\text{atm}}$  was likely the trigger of the onset of the Antarctic ice sheet, which then controlled the sea level changes (Miller et al., 2005). The EOT has been the most prominent climate transition of the whole Cenozoic, which highlights the important role of ice sheets in Earth's climate state (Westerhold et al., 2020).

The growth of the Antarctic ice cap took place in different steps and produced changes in global climate and ocean circulation. Oxygen and carbon isotopes of pristine marine carbonates can reveal important hints for paleoclimatology interpretations like temperature, isotopic ocean composition of seawater, dissolved organic carbon and changes in the carbon cycle, which may reflect productivity and atmospheric greenhouse gases (Marshall, 1992). Investigations

of stable isotopic composition of pristine marine carbonate showed variations in  $\delta^{13}\text{C}$  both in shallow-water and deep-sea, but most of the times regional and local factors are superimposed to the global forcing (Cornacchia et al., 2018). The transition into the Oligocene coolhouse world is documented by a rapid increase in benthic  $\delta^{18}\text{O}$  and  $\delta^{13}\text{C}$  records which is followed by a ~0.4 to 0.8-My-long recovery phase of decreasing  $\delta^{18}\text{O}$  and  $\delta^{13}\text{C}$  for the Early Oligocene (Pälike et al., 2006).

The aim of this thesis is to provide a new dataset for the Castelgomberto formation, a shallow water carbonate unit of Early Oligocene age that crops out in the Vicentinian pre-Alps, Northern Italy. One of the purposes of this study is to biostratigraphically date the succession, but also to use isotopic data to correlate, if possible, climate variations during this period to the overall stratigraphic evolution of the region.

## 1.1. Study area

The Berici Hills and Lessini Mountains are situated southward and westward with respect to Vicenza city, in the Northeast of Italy (Fig. 1). They cover an area of about 20x15 Km<sup>2</sup> and rise up to ~400 m over Quaternary deposits (Geister and Ungaro, 1977). They are located in the Southern Alps structural domain, which was partly involved in the Alpine deformation due to its constriction between the Giudicarie lineament to the west and the Schio-Vicenza fault to the east that enables the release of the Berici Hills and Lessini Mountains block during the deformation (Nebelsick et al., 2013).

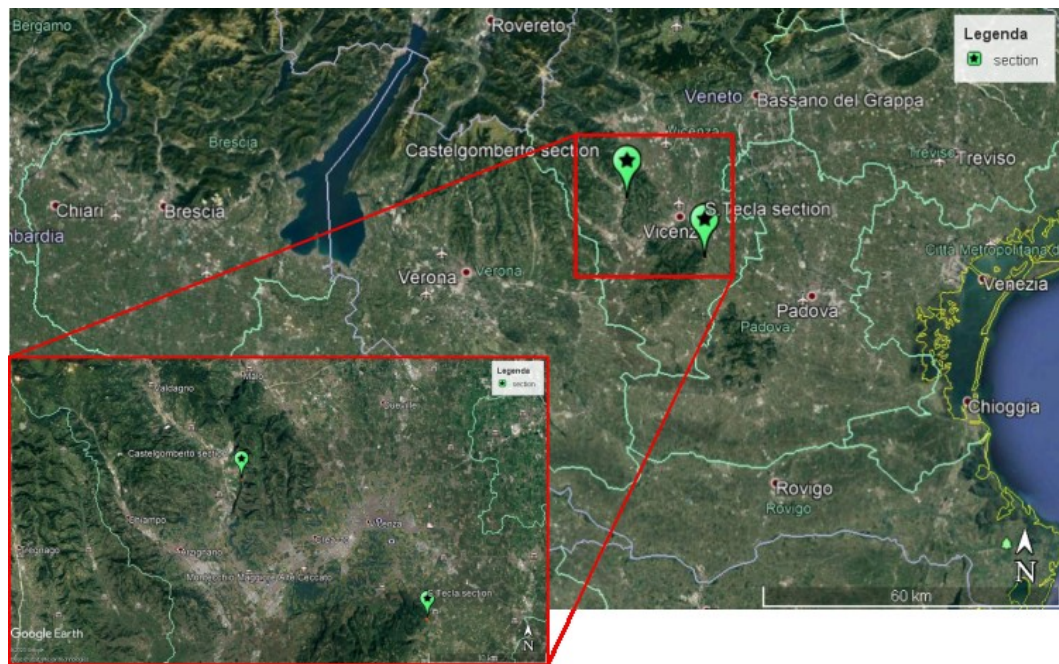


**Fig. 1: Berici Hills, Lessini Mountains and sections positions in the Northeast of Italy. Image from Google Earth.**

In the eastern Lessini Mountains, mafic and ultramafic eruptions occurred during the Late Paleocene- Late Eocene, mainly in submarine environment. During the Late Eocene, on the flanks of emerged volcanic ridges, marine transgressive sediments were deposited, the so called Priabona Formation ("*Marne di Priabona*" in De Vecchi et al., 1976).

The Priabona Formation is a shallow water carbonate unit which contains larger benthic foraminiferal and coralline algal assemblages. The formation deposited on a gently inclined ramp, thus offshore currents played an important role in both controlling substrates and supplying nutrients (Bassi, 2005).

Carbonates consists of wackestones, packstones, rudstones and bindstones dominated by coralline red algae and larger foraminifera. Accessory components comprise small benthic foraminifera, fragments of bryozoans, bivalves, echinoderms, rare solitary corals and serpulids.

The Priabona formation is underlain by the ~90 m thick Middle Eocene nummulitic limestone "*Calcari Nummulitici*" and overlain in the north-eastern and eastern part of Berici Hills by the lower Oligocene Castelgomberto formation (Bassi, 2005) (Fig. 2).

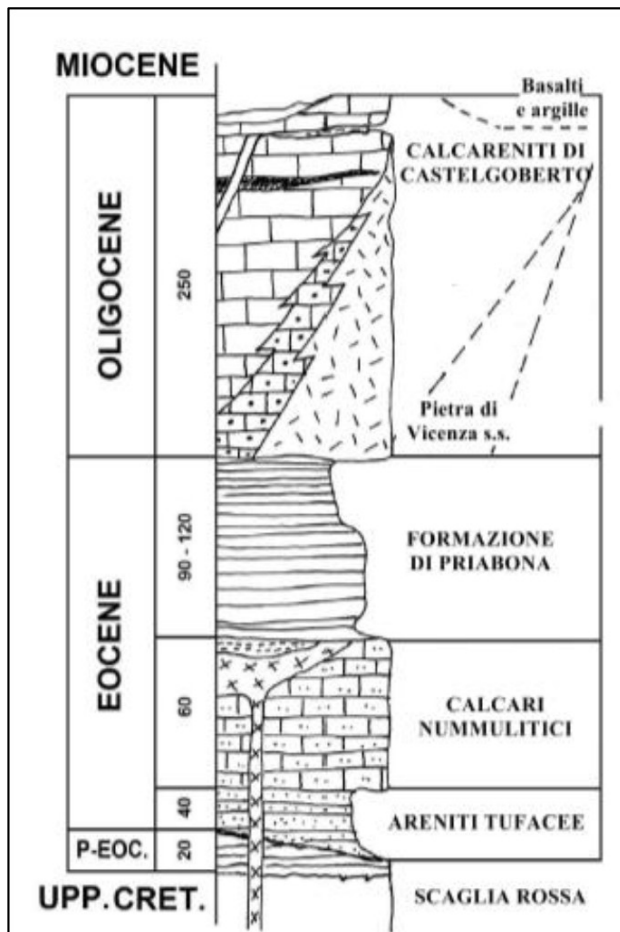


Fig. 2: stratigraphic section of Berici Hills. Image modified from Cornale et al. 1994

The volcanic activity continued in the Early Oligocene east of Schio, in the Berici and Euganei Hills (De Vecchi et al., 1976). After the Eocene, the tectonic activity controlled the accommodation space along with eustatic sea-level fluctuations and produced strong variations on sediment facies and thickness even on short distances. In the eastern Lessini Mountains and Berici Hills the lower Oligocene "Castelgomberto formation" deposited on the Priabona Formation, or directly on

the Bartonian volcanics where the Priabonian marls are missing (Márton' et al., 2011).

The Castelgomberto formation crops out over some 200 Km<sup>2</sup> in the hills of the eastern Lessini Mountains and in the Berici Hills. It mainly consists of highly fossiliferous wackestone to grainstone with local lignite beds and lenses of volcanic tuff or sedimentary breccia. In the south-eastern area of Berici Hills, Castelgomberto formation includes Oligocene barrier-reefs and/or carbonate shelf-edge buildups. In the rest of the Berici Hills, the basal Oligocene appears to be represented by skeletal limestones particularly enriched in nodular coralline algae. Earliest Oligocene sediments consists of beds of skeletal limestones rich in miliolid foraminifera and coralline algae alternating with marls and calcareous shales characterized by thickets of branching scleractinian corals. Oligocene rocks are also exposed in the Euganei Hills. These rocks are latitic-trachyandesite submarine flows, agglomerates, sedimentary tuffs and thin, fossiliferous marls (Frost, 1981).

In the Late Oligocene, the carbonate platform became emergent and affected by a deep paleokarst, testified in the whole region by cavities and dolines infilled by quartz sandstone (Frost, 1981). The unconformity is overlain by coralline algal rudstone ("Arenarie e Calcari di S.Urbano") of Late Oligocene age (Bassi et al., 2007).

Frost (1981) published a work on the paleoecologic distribution of reef corals and identified coral communities indicative of different environments. He described a 150-200 m thick barrier reef, 800-900 m wide and 8 Km long cropping out in the eastern Berici Hills (Fig. 3). Inside this barrier reef he identified three basic coral assemblages: lower diversity pioneers, high diversity reef-core and flank assemblages, which are indicative of protected habitats, and communities of soft mud substrates. The ecological features that drive the different distribution of

corals are: adaptation to water flow, potential to survive the rain of sediments, species-specific food related habits (Frost, 1981).

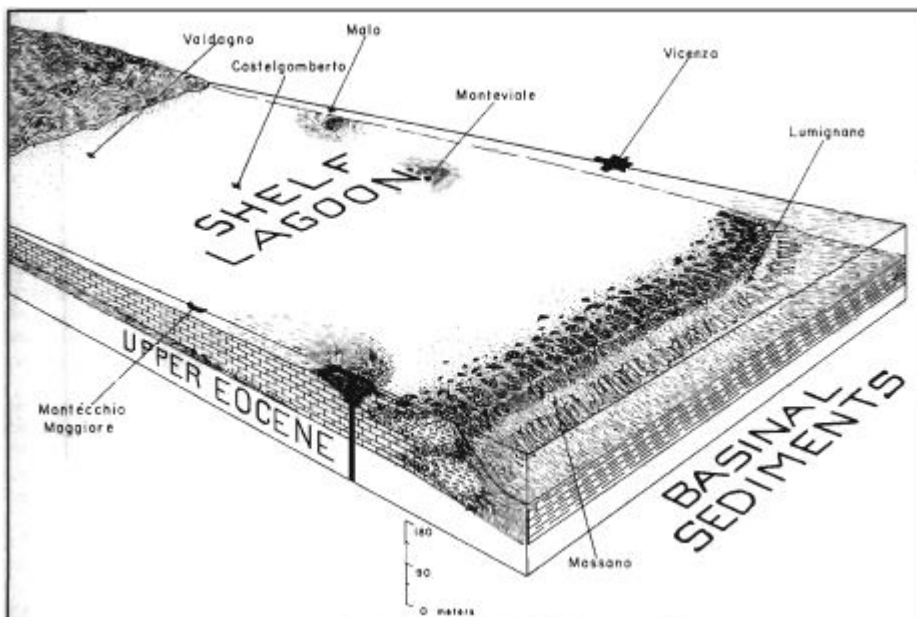
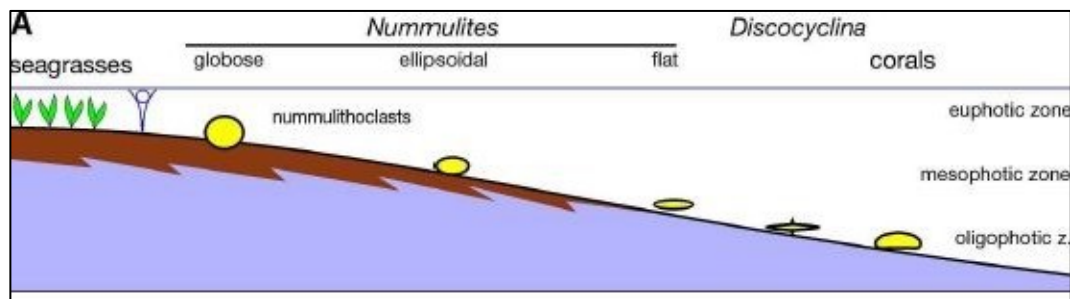


Fig. 3: Lessini carbonate platform scheme from Frost (1981)

This scheme remained the widely accepted interpretation for several years. The eastern edge of the Berici Hills is characterized by a scarp separating the hilly morphology of the Berici Hills (~500 m a.s.l.) from the flat alluvial deposits (starting at 30 m of elevation) of the Veneto plains. This morphological break, in fact, corresponds to a large fault, which essentially cuts off the transition from the Oligocene shallow water carbonates to the west to the basinal sediments to the east. The presence of this fault and the resulting lack of a gradual transition from shallow- to deeper-water deposits makes it difficult to assess if a rimmed shelf or a homoclinal ramp (or something in between) was present on the eastern edge of the Berici Hills (Nebelsick et al., 2013). Now, one possible interpretation for the depositional environment of Castelgomberto formation is that of a low angle ramp (homoclinal ramp) with alternating episodes of clay input; corals occur as isolated colonies along the whole ramp profile in the meso-

oligophotic zone. Seagrass meadow are interpreted to have occurred in the shallow euphotic part of the ramp (Pomar et al., 2017). A possible analog for the Castelgomberto formation may be the one presented by (Pomar et al., 2017)(Fig. 4).



**Fig. 4: A) Along-dip distribution of the carbonate factories in the Buil Level.** In the euphotic zone, epiphotic organisms thriving in seagrass meadows dominated carbonate production. The mesophotic zone was characterized by globose to ellipsoidal-flat *Nummulites* and, in the lower part, by coral biostromes. The oligophotic zone was dominated by large flat benthic rotalids (e.g., *Discocyclina*, *Nummulites millecaput*. Modified by Pomar (2017) from Mateu-Vicens et al. (2012).

Alternation of lithologies reflects changes in the composition of sediments deriving from inner and middle ramp, which can be explained by bathymetric variations, or by changes in the activity of carbonate factories, both related to climatic changes or sea-level cyclicity (Brandano et al., 2019).

Major changes of facies patterns at the Eocene-Oligocene boundary coincide with an extinction events among larger foraminifera (Nebelsick et al., 2005), in this area testified by the disappearance of genus *Discocyclina*. The Eocene-Oligocene transition corresponds to a significant sea-level drop of several tens of meters. A positive shift in benthic foraminifer  $\delta^{18}\text{O}$  values across Eocene-Oligocene Transition (EOT ~34 Ma) is widely interpreted as related mainly to the onset of major continental glaciation on Antarctica. From the biostratigraphic point of view, the E-O boundary is placed within calcareous nannofossil zone NP21 (Martini, 1971) or Subzone NP16a (Okada and Bukry, 1980). IT may be also set at the extinction of *Hantkenina* and *Cribrohantkenina* planktonic

foraminifera) within Chron C13r (Houben et al., 2012; Premoli, S. and Jenkins, 1933).

The study focuses on two sections where the Castelgomberto formation is well exposed:

-outcrop 1 in Castelgomberto town, Zaia Road (Fig. 5).

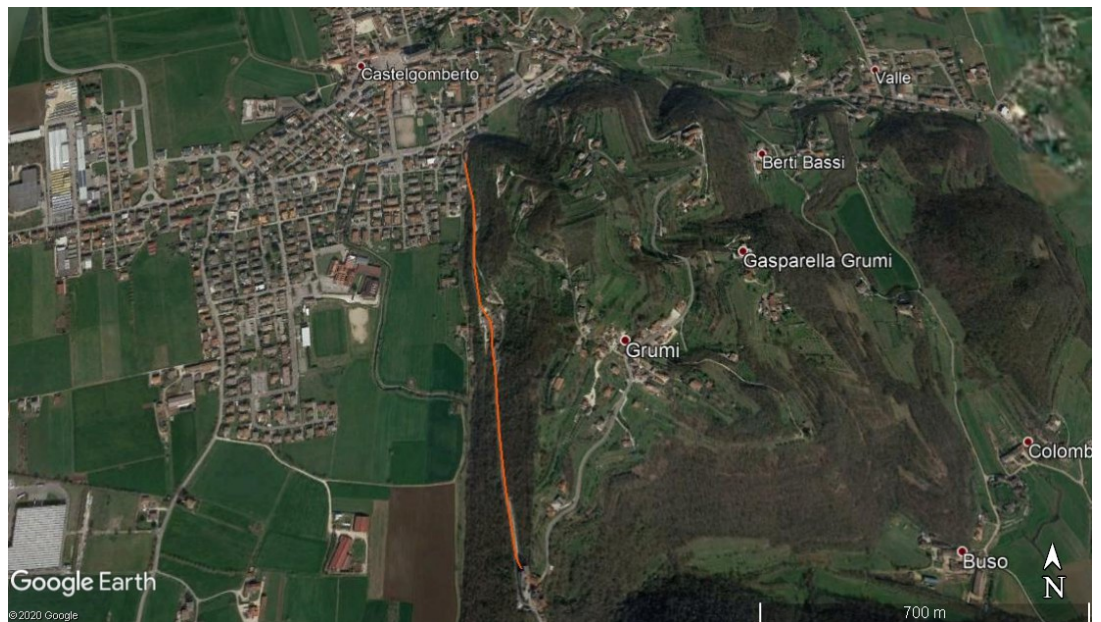


**Fig. 5: View of the Castelgomberto section. Image from Google Earth**

This locality was also investigated by Frost (1981) (Fig. 6).

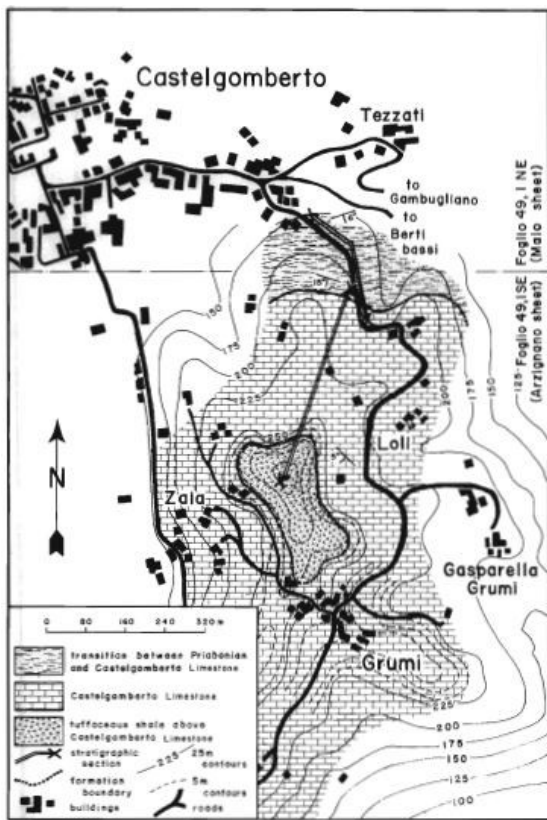


Fig. 6: Geologic map of Castelgomberto Monti Grumi area. Frost (1981)

-outcrop 2 in Costozza di Longare village, Santa Tecla Road (Fig. 7).



Fig. 7: view of Santa Tecla section. Image from Google Earth.

In particular, this section is characterized by coralline algal rudstones with a packstone to wackestone matrix. Algae are found in the form of encrusting thalli, rhodoliths and coralline debris. Non-algal components are larger/small benthic foraminifera, bryozoans, zooxanthellate corals and echinoderms (Nebelsick et al., 2013).

The Castelgomberto formation was dated to the lower Oligocene, and in both outcrops we are likely at the base of Early Oligocene, as previous studies recognized the horizon of "Pietra di Vicenza" that locally marks the base of the stage. This horizon lies at the base of both outcrops 1 and 2 (Milizia, 2019). The biostratigraphic classification of the S.Tecla section is based on the presence of the larger foraminifera *Nummulites fichteli*, *N. vascus*, *Operculina complanata*, *Praerhapydionina delicata*, *Spirolina cylindracea*, *Peneroplis glynnionesi* and *Asterigerina rotula haeringensis* (Nebelsick et al., 2013). These larger

foraminifera constrain the sections to zones SB21-22A (Rupelian) (Cahuzac and Poignant, 1997).

One of the goal of this study is to date the middle-upper part of this unit, that is eventually overlain by S.Urbano limestone, which has a Chattian age (Late Oligocene).

## 2. METHODS

The Castelgomberto formation has been logged and sampled for petrographic observations, biostratigraphy and stable isotopic analyses. The upper part of Castelgomberto section was sampled and studied in a previous master thesis (Cherobin, 2015): in this thesis, we have integrated that part with newly collected samples. The Santa Tecla section, instead, has been part of some important studies and reconstructions (Nebelsick et al., 2013) but we have completely re-sampled it for this study.

### 2.1. Sample collection

We have sampled the Castelgomberto section for the petrographic identification of microfacies. Thin sections were observed at a petrographic microscope, thus samples from each facies have been collected along the section. We also collected specimens of oysters and pectinids for isotope analysis, when possible, these will be discussed later in the text. At Castelgomberto, we also recognized some clay-rich layers. According to Pomar et al. (2017), these layers formed in the deepest part of the ramp profile, and could thus contains planktonic microfossils such as foraminifera or calcareous nannofossils (Fig. 8).



**Fig. 8: map of Castelgomberto sections with samples collected. "N" marks are for nannofossil samples, "O" marks for oysters and pectinids samples and "S" marks for thin section samples. Image from Google Earth.**

In the Castelgomberto section, we collected six oysters, two pectinids, fifteen rock samples and ten clay-rich samples for nannofossil analysis.

In the Santa Tecla section, the aim of the sampling was partially different. We sampled for oysters and pectinids, but we also collected rock samples for a stable isotopic analysis on bulk. Finally, we sampled clay-rich layers for calcareous nannofossils (Fig. 9).



**Fig. 9:** map of Santa Tecla section with samples collected. "N" marks for nannofossil samples, "O" marks for oysters and pectinids samples and "B" marks for rock bulk samples.

In the Santa Tecla section, we collected six oysters, three pectinids, fifty-one rock samples and six clay-rich samples for nannofossil analysis.

## 2.2. Calcareous Nannofossils

Clay-rich samples have been scraped to expose a fresh surface, then a small clean portion of the sample was collected with a lancet.

Clays-rich samples have been gently washed and then dried for two hours in an oven at 40°C. After drying, the surface of the sample has been removed to collect an uncontaminated sample, which has been then scraped and powdered on a slide. The powder has been mixed to a drop of deionized water with a straw and then smear on the slide. We dried the smear slide over a heating plate at 100°C for few seconds, then glued the cover slip. The optical adhesive Norland used is a particular glue which hardens after 10 minutes under UV light. All tools have

been washed with HCl 10% and rinsed with deionized water before operating again.

We analyzed the smear slides under a ZEISS optical microscope (x1250 magnification) with X100 oil immersion lens, we used Immersol 518N ISO8036, he=1.518 (23°C) Ve=42 as oil. Three vertical transects on each smear slide have been counted and then normalized the counting to 1 mm<sup>2</sup> (which corresponds to 50 Fields of View in the microscope used).

The biostratigraphic scheme adopted are those of Martini (1971), Okada and Bukry (1980) and Agnini et al. (2014).

## **2.3. Isotopic sample preparation and analysis**

$\delta^{13}\text{C}$  and  $\delta^{18}\text{O}$  were measured on bulk rock samples, and on the oysters and pectinids (bivalves) collected in the field. For the Castelgomberto section, eight samples from the upper part of the section, that were collected for a previous master thesis (Cherobin, 2015), have been added to those collected for this thesis. We also added one sample from "Cava Valle" quarry, where "Pietra di Vicenza" crops out, which is positioned right below the base of the study section. In the Santa Tecla section, four samples were taken from the horizon of "Pietra di Vicenza" below the study succession (Covolo Carli in Fig. 10).



**Fig. 10:** map of samples from "Pietra di Vicenza" horizon below the study succession of Santa Tecla. Image from Google Earth.

Bivalve samples have been washed and gently rubbed, then rinsed in deionized water and dried in an oven at 40°C for 2 hours. We used a dentist drill with tungsten carbide tip to produce powders. When possible, we drilled more than one spot, and according to the size of the sample, we tried to separate fibrous layers and prismatic layers in oysters. In oysters, fibrous layers are made of low-Mg calcite, and have thus a higher potential to preserve the pristine isotopic signal (e.g., Hasiuk et al., 2016). These layers are recognizable under transmission microscope or by their darker color. During thin sections preparation, we found more specimens of calcitic bivalves that were also drilled. A small amount (< 1 g) of powder was produced and placed in a Eppendorf capsule for each sample. The tip of the drill was cleaned in HCl 10% and then rinsed in deionized water, and each sample was clean with compressed air, before the sampling.

Rock samples collected in the Santa Tecla section have been used for bulk analysis. A chip of each sample was ground in an agate mortar (Fig. 11). Chips were obtained with a crusher.

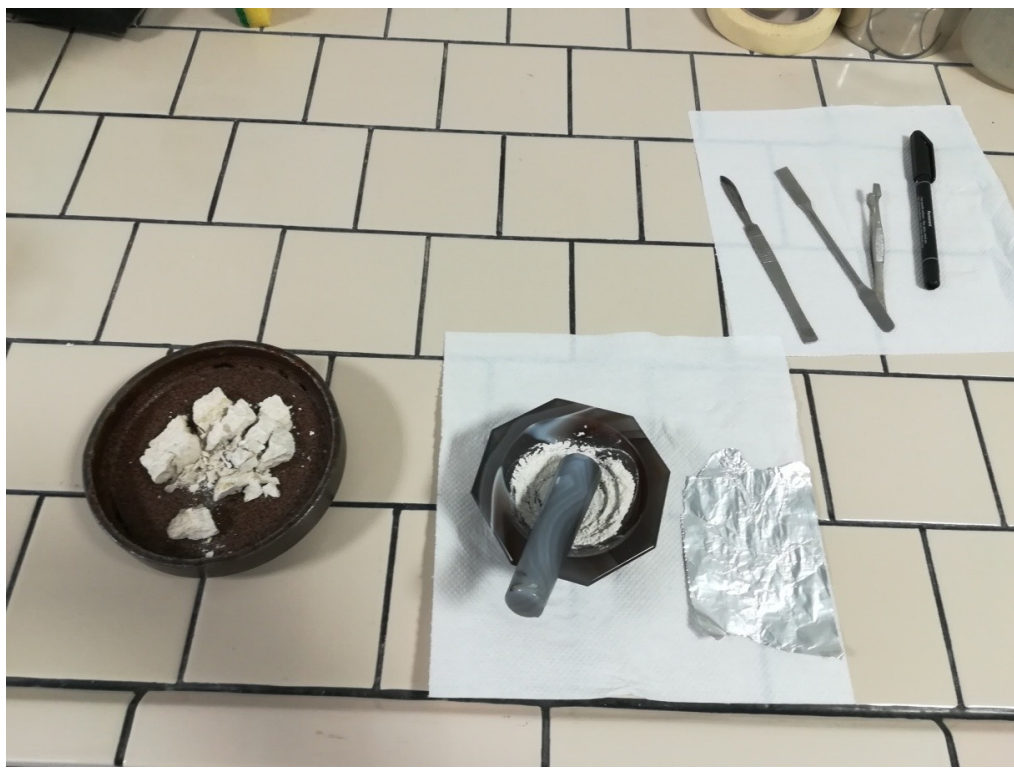


**Fig. 11: For bulk analysis the chips obtained with a crusher have been ground in an agate mortar.**

Bulk powder has been also produced from the same samples by using a dentist drill with tungsten carbide tip. To ensure that the powder is representative of the rock, five holes have been drilled in straight line across each sample. This double sampling was done in order to test the reliability of the sampling by dental drill, which is far less time consuming than grinding in a mortar, in the case of the rudstone facies of Santa Tecla, which are highly heterogeneous.

Rock leftovers from thin sections of the Castelgomberto section have been drilled for bulk analysis as well.

Powdered samples were weighted with a precision balance for the mass spectrometer analysis. The weight of samples ranged from 0.180 to 0.500 mg, ideally 0.200-0.350 mg. The powder was then placed in a test vial and closed with a plastic cap. When running the samples, in-house standard samples were

added: MAQ1, is an in-house standard made of pure Carrara marble and calibrated periodically with NBS19 international standard. The nominal values of MAQ1 are  $\delta^{13}\text{C}=2,58\text{\textperthousand}$  and  $\delta^{18}\text{O}=-1,15\text{\textperthousand}$  VPDB. A second standard, GR1, was included in the run as quality control standard. GR1 is a pure marble collected at the San Pellegrino Pass and has values of  $\delta^{13}\text{C}=0,68\text{\textperthousand}$  and  $\delta^{18}\text{O}=-10,44\text{\textperthousand}$  VPDB. Both standards are powdered and then sieved, the used fraction is 80-150  $\mu\text{m}$ .

For bulk analysis, in addition to the standards for calibration and quality control (i.e., MAQ1 and GR1), we added a series of MAQ1 with variable weights. These standard samples produced peaks that vary in function of the carbon content, and allow to estimate the amount of carbonate in the rock (sample) (Spofforth et al., 2010).

The mass spectrometer used for analysis is located in the Department of Geosciences of the University of Padua. Specifically, this is a Delta V Advantage (Thermo Scientific) connected with a Gasbench II device for the development of CO<sub>2</sub> gas from carbonates (Fig. 12). The test vials containing the samples were placed in the Gasbench box. A mechanical arm with syringe introduced Helium in the test vials to remove air, and then orthophosphoric acid (>99%) has been injected manually, and the reaction with carbonates is allowed to continue for at least 3 hours, at 70°C. After this time, the gas is extracted from the vial and sent to the chromatographic column and then analyzed by the spectrometer.



**Fig. 12:** Mass spectrometer Delta V Advantage (Thermo Scientific) connected with a Gasbench II device. Department of Geosciences, University of Padua.

## 3. Results

These results presented in the following chapter have been collected from the processing of all the samples collected during this thesis work, plus the samples coming from previous studies and already mentioned above.

### 3.1. Nannofossils

The abundance pattern of marker index species has been analyzed. In particular the biohorizons used to subdivide the interval of interest are: Top of *Ericsonia formosa* (32.92 Ma), Base common (acme beginning) of *Clausicoccus subdistichus* (33.88 Ma), Base of *Dictyococcites bisectus* (size > 10 $\mu$ m)(40.34 Ma), Top of

*Reticulofenestra umbilicus* (size > 14 $\mu$ m)(32.02 Ma), Top common of *Cribrocentrum reticulatum* (35.24 Ma), Top of *Discoaster saipanensis* (34.44 Ma), Top of *Discoaster Barbadiensis* (34.77 Ma) and Base of *Sphenolithus distentus* (30 Ma) (Agnini et al., 2014). Biochronological estimates are after Agnini et al. (2014), calibrated to GTS 2014.

After counting 3 slide transects and normalizing to 1 mm<sup>2</sup>, we reported the results into graphs to have a clearer view of the abundance patterns of each single species along the sections (depth in m).

For the Castelgomberto section, the total number of nannofossils/mm<sup>2</sup> and number of reworked nannofossils/mm<sup>2</sup> are reported in light blue, while the semi-quantitative abundances of the index species are reported in magenta (Fig. 13). All the other species are in black (Fig. 14). Note that the order of the plot is a function of the abundance (mm<sup>2</sup>).

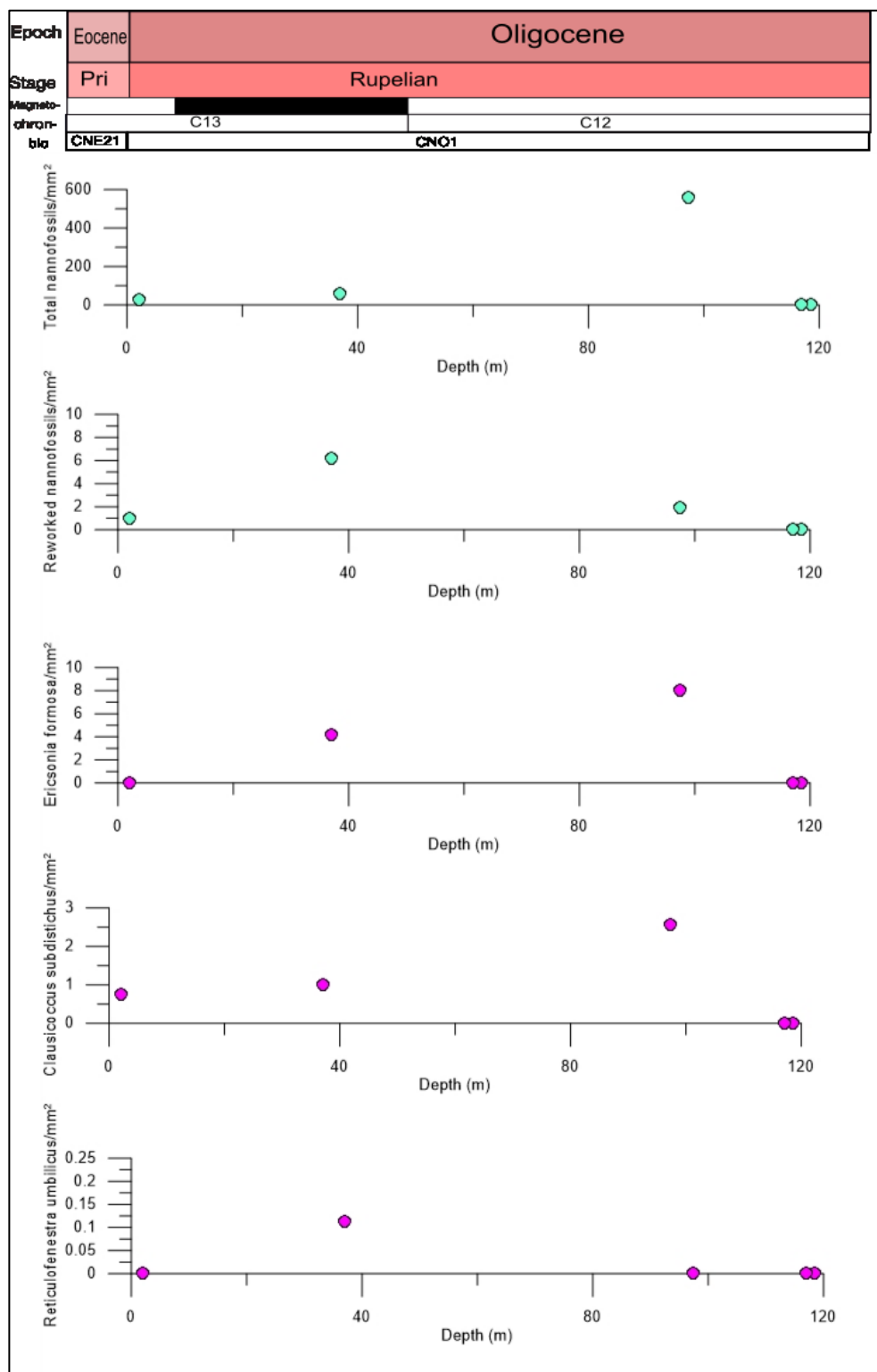


**Fig. 13:** Castelgomberto total number of nannofossils/mm<sup>2</sup> and number of reworked nannofossils/mm<sup>2</sup> are reported in light blue, the semi-quantitative abundance of the index species (*Ericsonia formosa*, *Clasicoccus subdistichus*, *Reticulofenestra umbilicus*) are reported in magenta.

Out of the ten samples collected, four samples were barren of nannofossils and two display a very low preservation and were not further investigated. Out of the four analyzed samples, only two contained marker species and were used to biostratigraphically constrain the study section.

Among reworked nannofossils found in this sections, we list here some of them: *Biantholithus*, *Braarudosphaera*, *Chiasmolithus solitus*, *Coccolithus crassus*, *Cribrocentrum erbae*, *Cribrocentrum reticulatum*, *Discoaster barbadiensis*, *Discoaster tanii*, *Helicosphaerae*, *Micula*, *Prediscosphaera*, *Toweius*, *Watznaueria* etc.

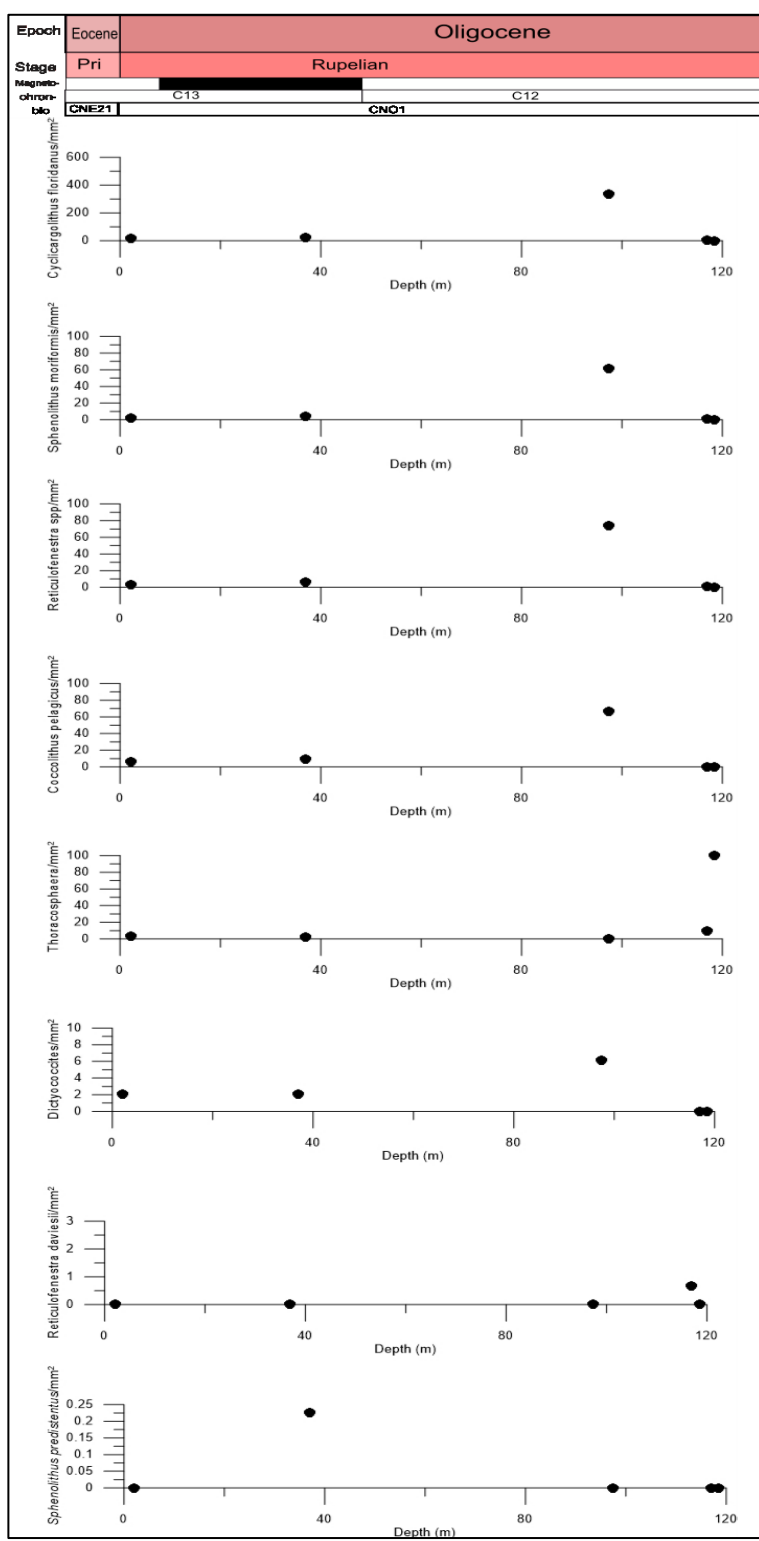


**Fig. 14:** from the top *Cyclicargolithus floridanus*, *Sphenolithus moriformis*, *Reticulofenestra* spp., *Coccolithus pelagicus*, *Thoracosphaerae* spp., *Dictyococcites*, *Reticulofenestra daviesii*, *Sphenolithus predistentus*.

Overall, samples had a very low to moderate preservation and the one (FCCN08) with the best preservation also contains a very high number of reworked specimens (for all details see appendix: Tab. 1).

For the Santa Tecla section, the total number of nannofossils/mm<sup>2</sup> and number of reworked nannofossils/mm<sup>2</sup> are reported in light blue, while the semi-quantitative abundances of the index species are reported in magenta (Fig. 15). All the other species are in black (Fig. 16). Note that the order of the plot is a function of the abundance (mm<sup>2</sup>).

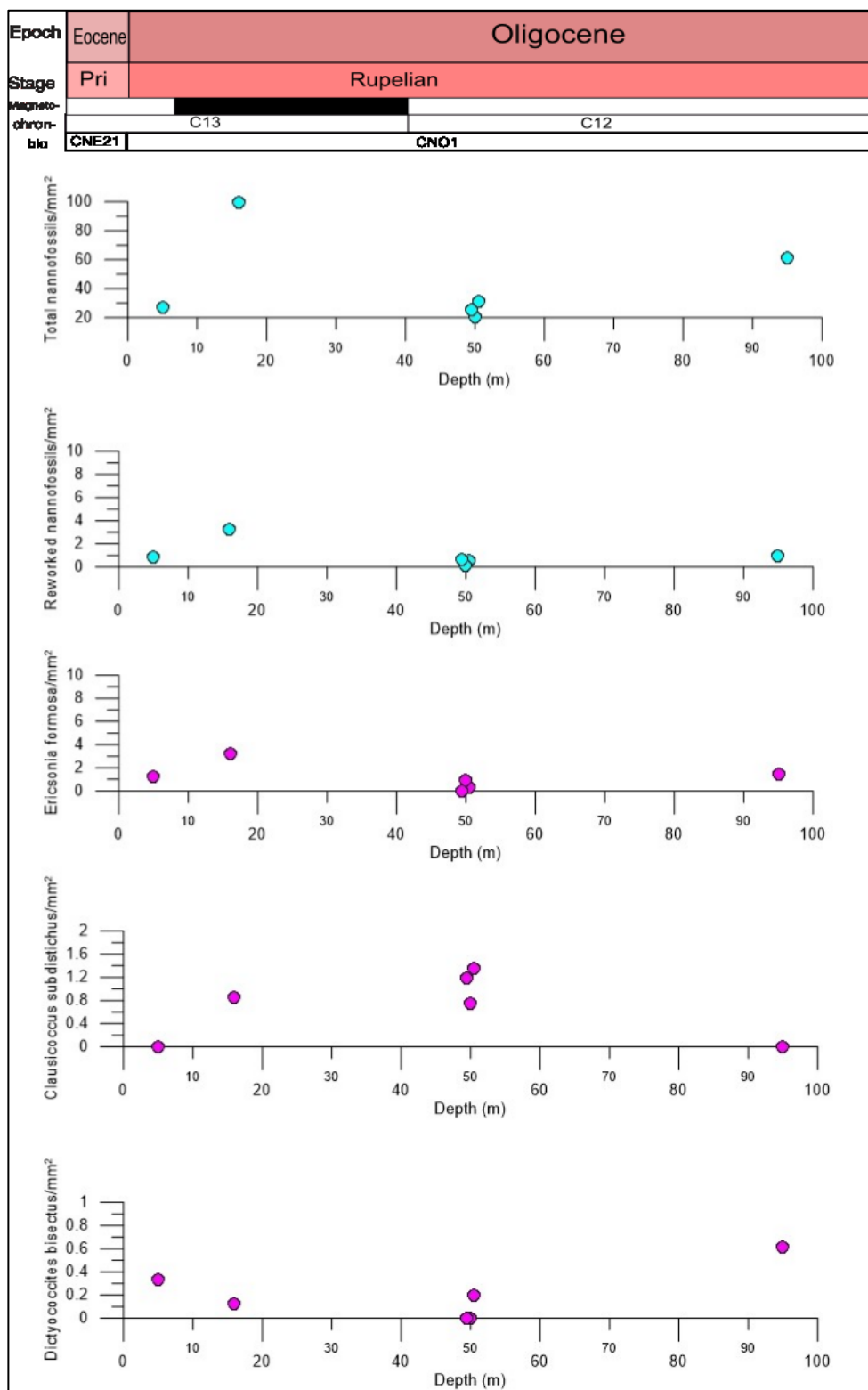


**Fig. 15:** Santa Tecla total number of nannofossils/mm<sup>2</sup> and number of reworked nannofossils/mm<sup>2</sup> are reported in light blue, the semi-quantitative abundance of the index species (*Ericsonia formosa*, *Clausicoccus subdistichus*, *Dictyococcites bisectus*) are reported in magenta

All the samples collected contained calcareous nannofossils, the presence of index species allows to constrain the section biostratigraphically.

The samples contained some reworked nannofossils such as: *Biantholithus*, *Chiasmolithus solithus*, *Cribrocentrum reticulatum*, *Discoaster tanii*, *Sphenolithus anarrhopus*, *Retecapsa*, etc.

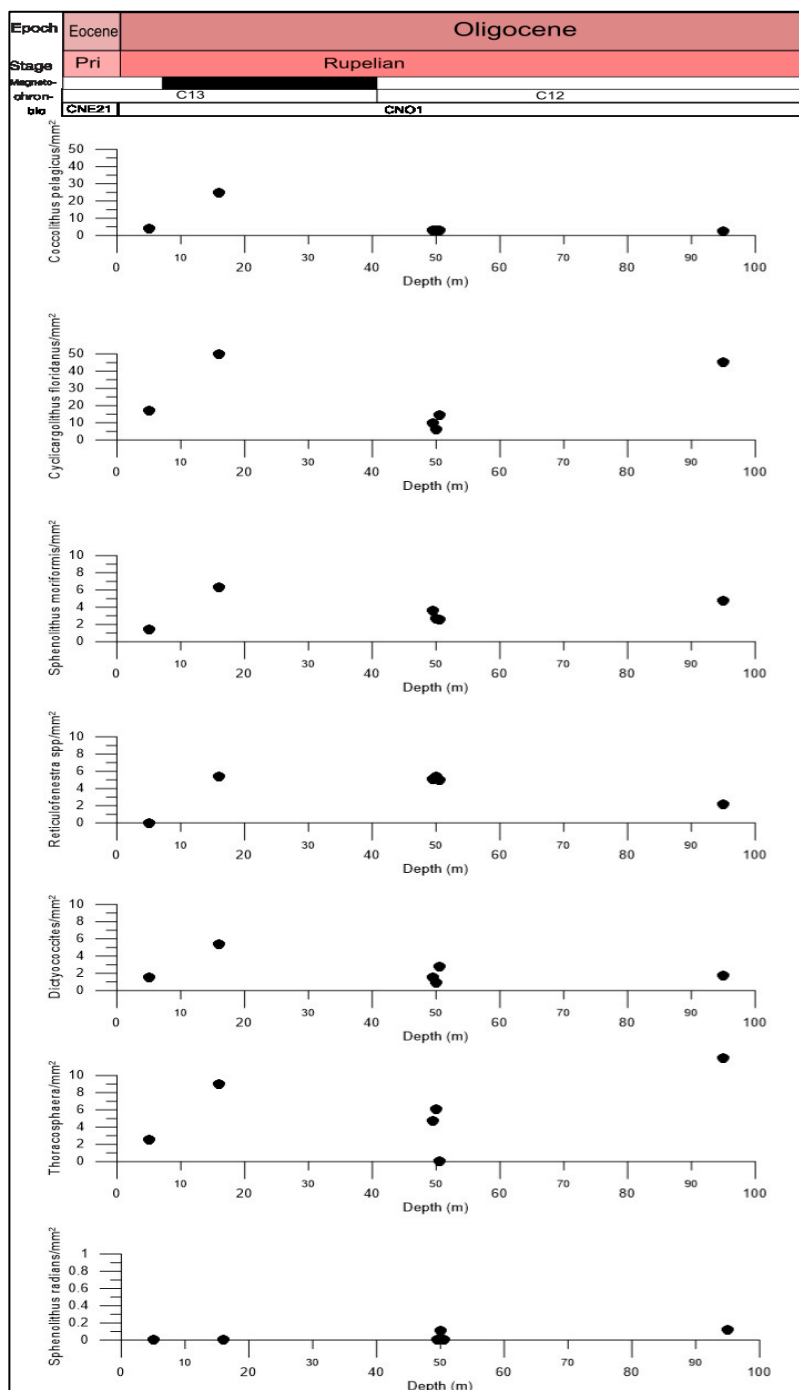


**Fig. 16:** from the top *Coccolithus pelagicus*, *Cyclicargolithus floridanus*, *Sphenolithus moriformis*, *Reticulofenestra spp.*, *Dictyococcites spp.*, *Thoracosphaera spp.*, *Sphenolithus radians*.

The preservation varies from low to moderate/low (for all details see appendix:  
Tab. 2).

### **3.2. Facies of the Castelgomberto formation**

From the Castelgomberto section, two logs have been made (Fig. 19 and Fig. 20), in addition the upper portion that was logged during a previous thesis (Cherobin, 2015)(Fig. 21) and the lower part (Cava Valle quarry) from another thesis (Milizia, 2019)(Fig. 22). Thin sections have been observed and the facies have been uniformed as follows:

- Facies A (Fig. 18\_A): red algae and nummulitids rudstone. Main components: coralline and encrusting red algae, rhodoliths, nummulitids. Other components: hyaline and agglutinated benthic foraminifera, echinoderms, bryozoans, gastropods and bivalves (Fig. 17). Massive bedding with wavy amalgamated joints.
- Facies B (Fig. 18\_B): red algae floatstone. Main components: encrusting red algae. Other components: oysters, bryozoans, serpulids and barnacles (Fig. 17). Nodular layering with abundant clay.
- Facies C (Fig. 18\_C): red algae and coral floatstone with wackestone matrix. Main components: corals, red algae, nummulitids and miliolids. Other components: gastropods and small benthic foraminifera (Fig. 17). Reef corals may occur into a clay matrix. Corals form an unbound continuous uniform mixstone (according to Insalaco, 1998).
- Facies D (Fig. 18\_D): Miliolids packstone-grainstone. Main components: miliolids. Other components: mollusks and other skeletal grains (Fig. 17). Well stratified, with wavy joints, almost nodular at a dm scale.
- Facies E (Fig. 18\_E): fine skeletal wackestone-packstone. Main components: fragmented skeletal grains and planktonic foraminifera (Fig. 17).

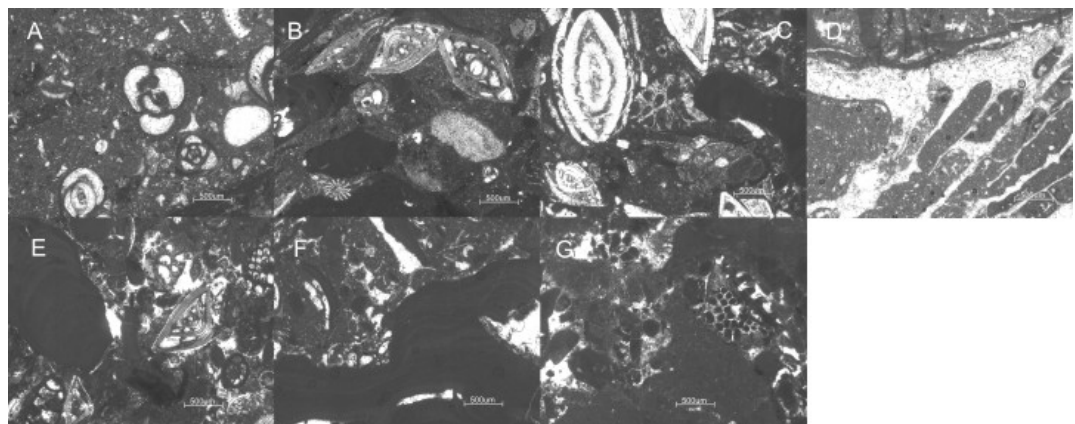


**Fig. 17:** photo of rock components, from the Castelgomberto section. A) sample C from top Castelgomberto section, m 77, with miliolids, facies C; B) sample FCC01 from base Castelgomberto section, m 1.5, with nummulitids, red algae and echinoderms, facies A; C) sample FCC02 from base Castelgomberto section, m 4.5, with nummulitids, foraminifera and bryozoans, facies C; D) sample P top Castelgomberto section, m 107.5, with corals, facies C; E) sample FCC03 base Castelgomberto section, m 7, with nummulitids, branching red algae, small benthic foraminifera and bryozoans, facies A; F) sample FCC05 base Castelgomberto section, m 10, with rhodoliths and bivalve, facies A; G) sample FCC09 from base Castelgomberto section, m 19, with bryozoan, facies C.

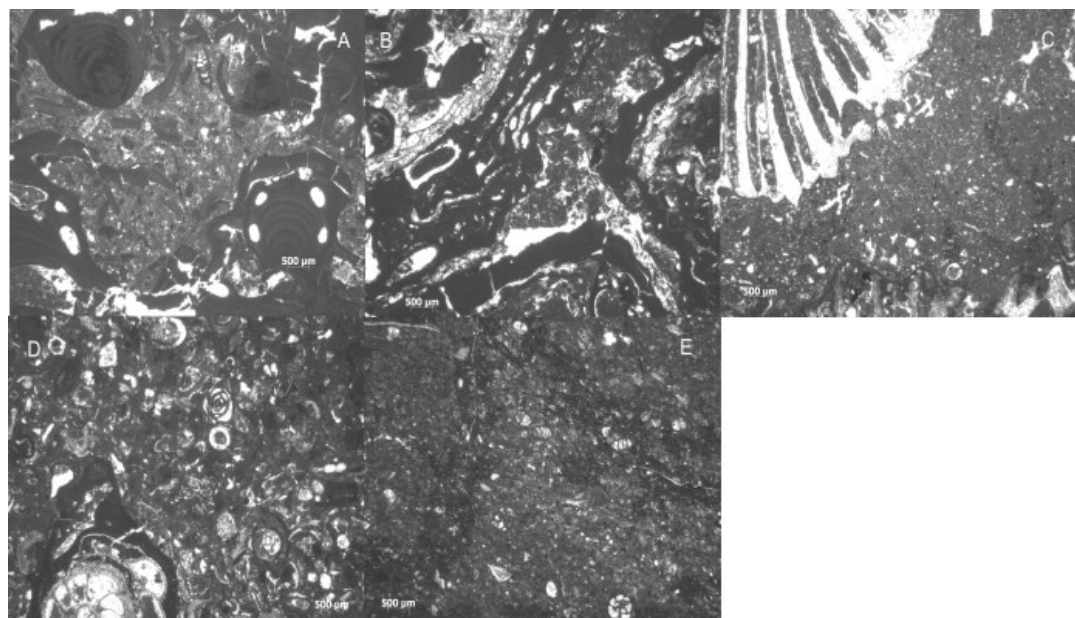


**Fig. 18:** photo of facies in this section, from the Castelgomberto section. A) Facies A: sample FCC05 from base Castelgomberto section, m 10, with branching coralline red algae and small benthic foraminifera. B) Facies B: sample FCC04, from base Castelgomberto section, m 8.5, with rhodoliths. C) Facies C: sample P from top Castelgomberto section, m 107.5, with corals. D) Facies D: sample G from the top of Castelgomberto section, m 89, with miliolids, gastropods and skeletal grains. E) Facies E: sample N from the top of Castelgomberto section, m 106, with small benthic foraminifera and other fine skeletal grains.

# CASTELGOMBERTO

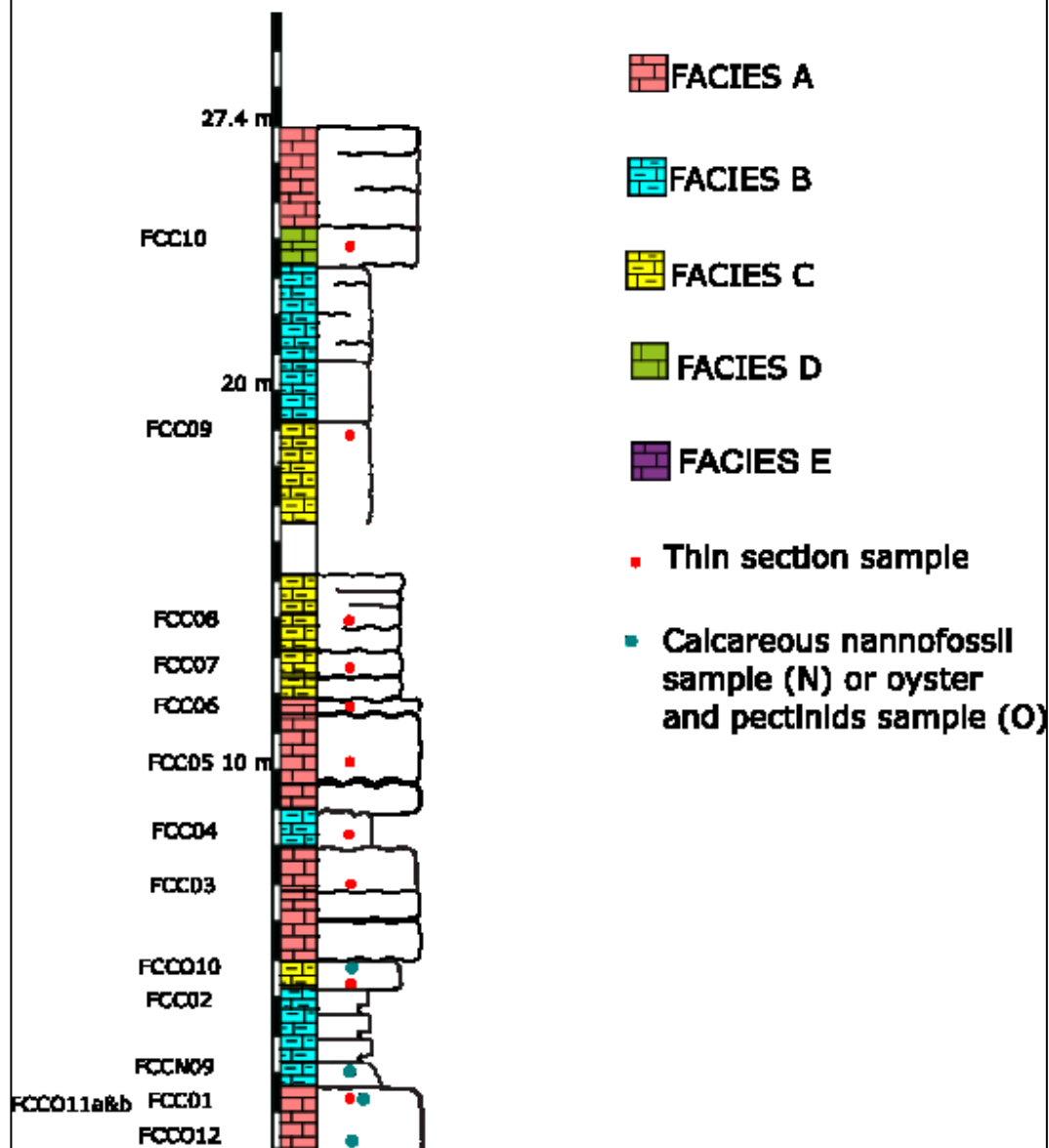


Fig. 19: Log from the base of section at Castelgomberto. Red dots are for thin section samples, blue dots are for other samples recognizable by letters: N for nannofossil, O for oysters and pectinids.

# "Casa Mazzago"

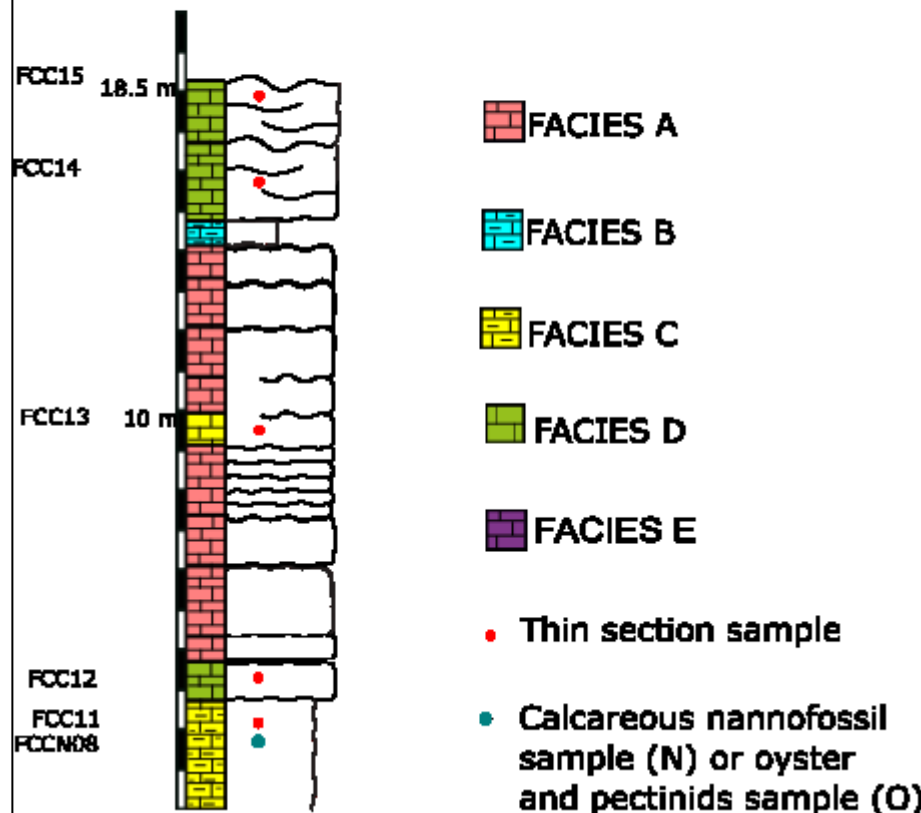


Fig. 20: Log of the intermediate part of section at Castelgomberto. Red dots are for thin section samples, blue dots are for other samples recognizable by letters: N for nannofossil, O for oysters and pectinids.

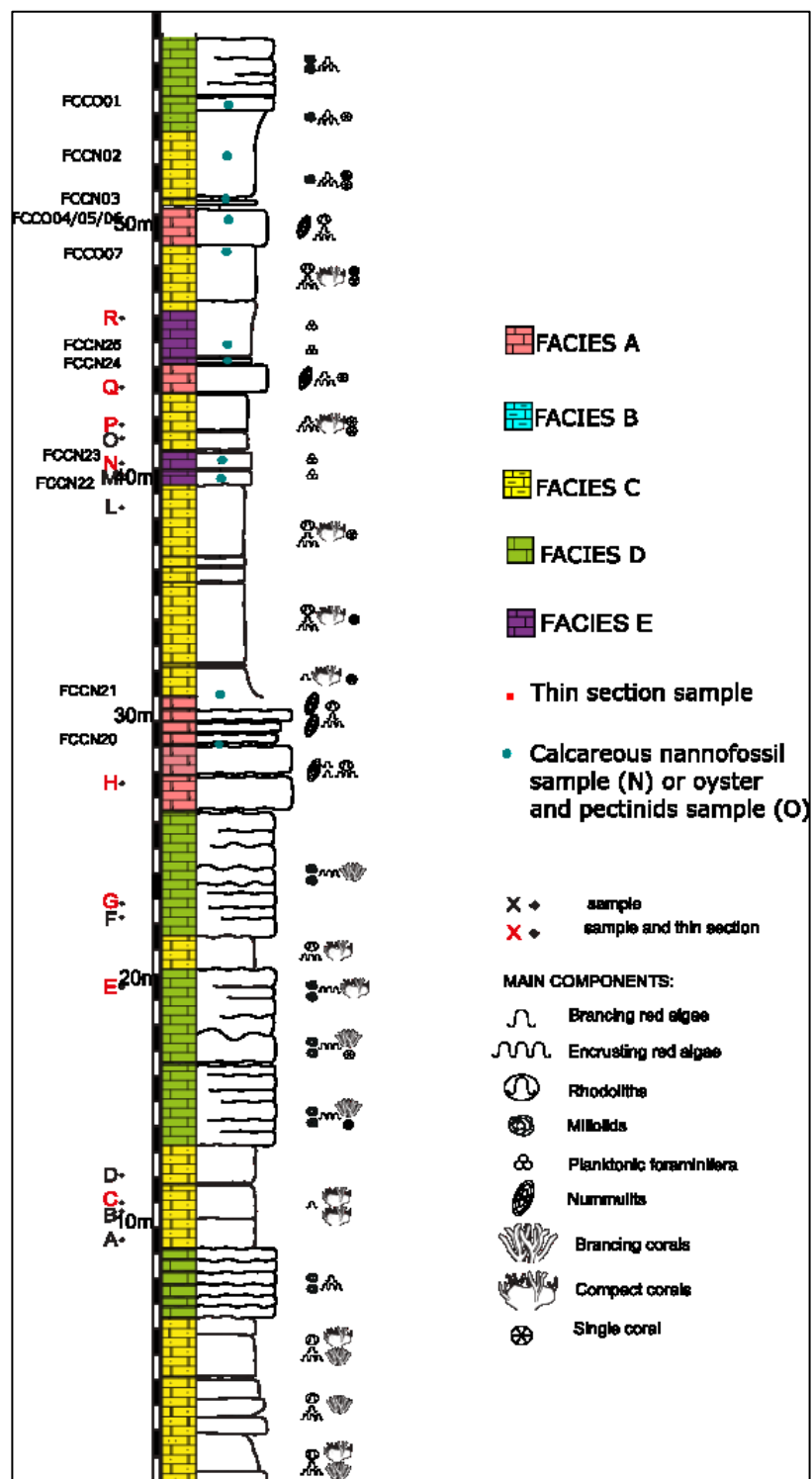


Fig. 21: Log of the upper part of our section (Cherobin, 2015). Red dots are for thin section samples, blue dots are for other samples recognizable by letters: N for nannofossil, O for oysters and pectinids. Thin sections were made from red letters samples which are also the samples we drilled for bulk isotope analysis.

CAVA VALLE

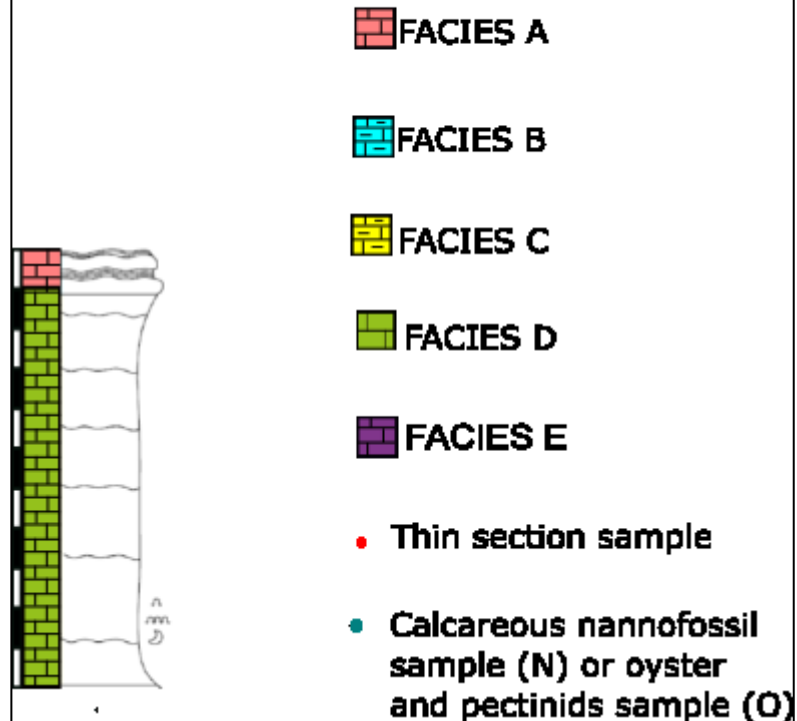


Fig. 22: Log of Cava Valle, a Pietra di Vicenza quarried horizon, from Milizia (2019).

For the S.Tecla section the log used comes from Nebelsick et al. (2013) (Fig. 23).

Facies along the section have been observed and uniformed to the others.

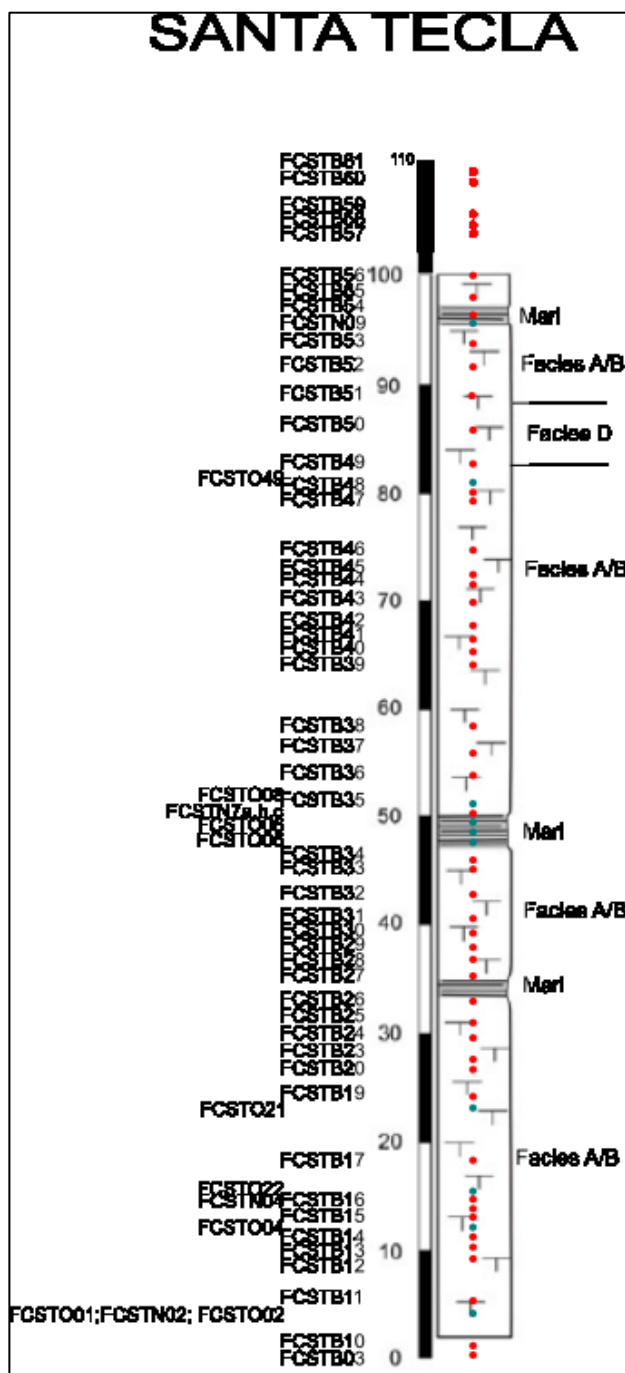


Fig. 23: Log of the Santa Tecla section modified after Nebelsick et al. (2013) with the samples collected. Red dots are for thin section samples, blue dots are for other samples recognizable by letters: N for nannofossil, O for oysters and pectinids.

Log of Covolo Carli, from Maruzzo (2019). Also for this log, facies were relabeled to be uniform with our classification (Fig. 24). Samples 1-4 are the ones drilled for isotope bulk analysis in this study.

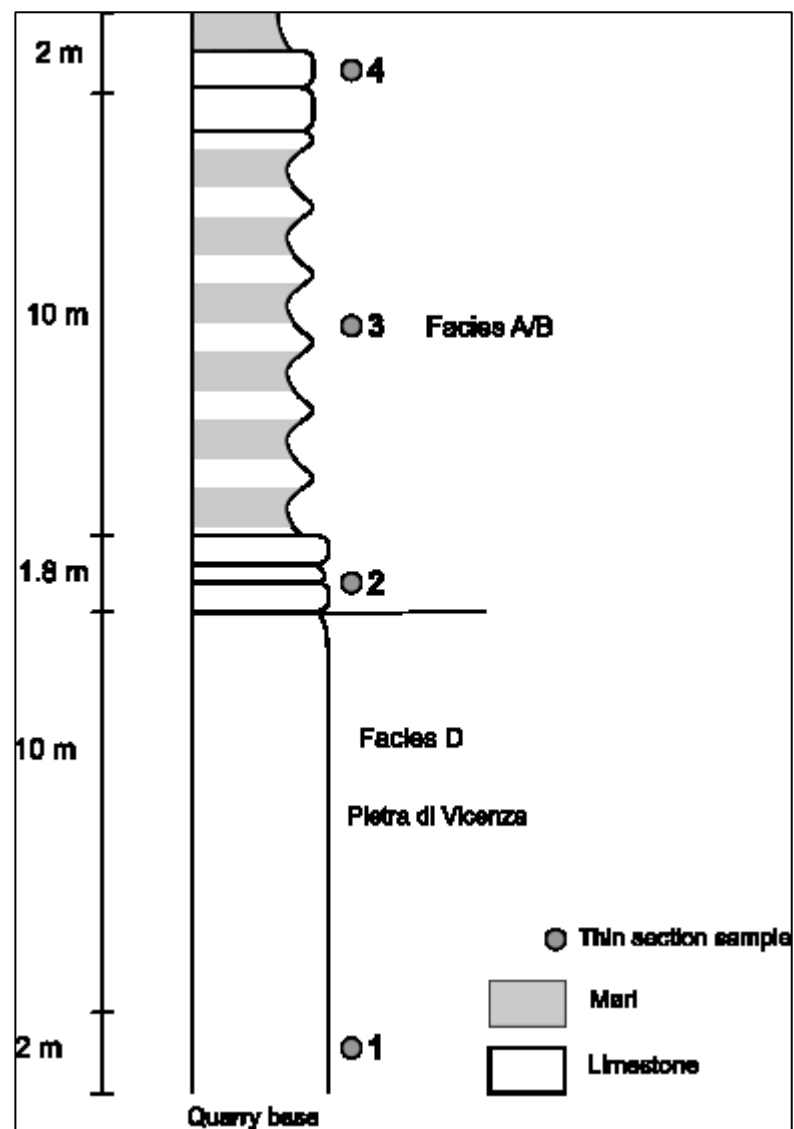
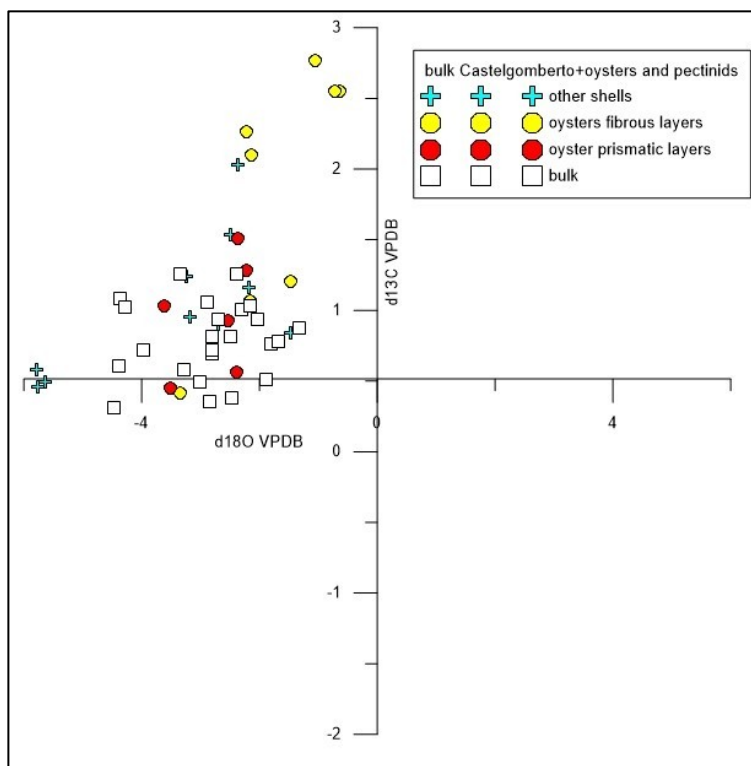


Fig. 24: log from Covolo Carli From Maruzzo (2019) and samples drilled for bulk analysis in this study.

### 3.3. Carbon and oxygen stable isotope data

The results of stable isotopic analysis of carbon and oxygen are presented via cross plots.

Figure 25 is a cross plot of Castelgomberto  $\delta^{13}\text{C}$  vs  $\delta^{18}\text{O}$  VPDB values of drilled bulk samples of Castelgomberto and Cava Valle, plotted together with those of oysters and other shells (i.e. pectinids and shells from thin sections).



**Fig. 25:** Cross-plot of isotopic results from the Castelgomberto section  $\delta^{13}\text{C}$  vs  $\delta^{18}\text{O}$  VPDB values of drilled bulk samples from the Castelgomberto section and Cava Valle quarry (white squares) are plotted together with those of oysters (yellow dots for low-Mg calcite fibrous-layers and red dots for prismatic layers) and other shells (i.e. pectinids and shells from thin sections)(light blue crosses).

Fibrous oyster layers (i.e. low-Mg calcite) better preserved the pristine isotopic signal if compared with other shells and prismatic oyster layers samples. This interpretation is supported by the fibrous layers having less negative values, thus suggesting that diagenetic processes were absent or at least modified the oxygen

isotopic composition of the fibrous shell layers only minimally (Hasiuk et al., 2016). Isotopic bulk analysis shows values between -1 and -5‰ VPDB for  $\delta^{18}\text{O}$  and between -1 and 1.5‰ VPDB for  $\delta^{13}\text{C}$  (for all details see appendix Tab. 3 and Tab. 4).

The total dataset consists of by 24 oysters samples and 24 bulk samples. A t-test for independent samples has been made to determine if there is a difference between the means of the two groups at a standard significance threshold of 95%. We assume a normal distribution of the values without outliers. Mean  $\delta^{13}\text{C}$  VPDB for oysters is 1.29 ‰ with standard deviation of 0.73 ‰, while the mean  $\delta^{13}\text{C}$  VPDB for bulk is 0.79 ‰ with a standard deviation of 0.27 ‰. The difference between means is 0.5 ‰, which is very statistically significant with  $t(46) = 3.1471$ ;  $p\text{-value} = 0.0029$ . "t(46)" stands for a t statistic with a 46 degrees of freedom (the degrees of freedom being equal to the number of samples, minus 2).

$\delta^{13}\text{C}$  vs  $\delta^{18}\text{O}$  VPDB plots of bulk samples from the S.Tecla section and Covolo Carli are displayed together with oyster and "other shells" samples (i.e. pectinids) in figure 26.

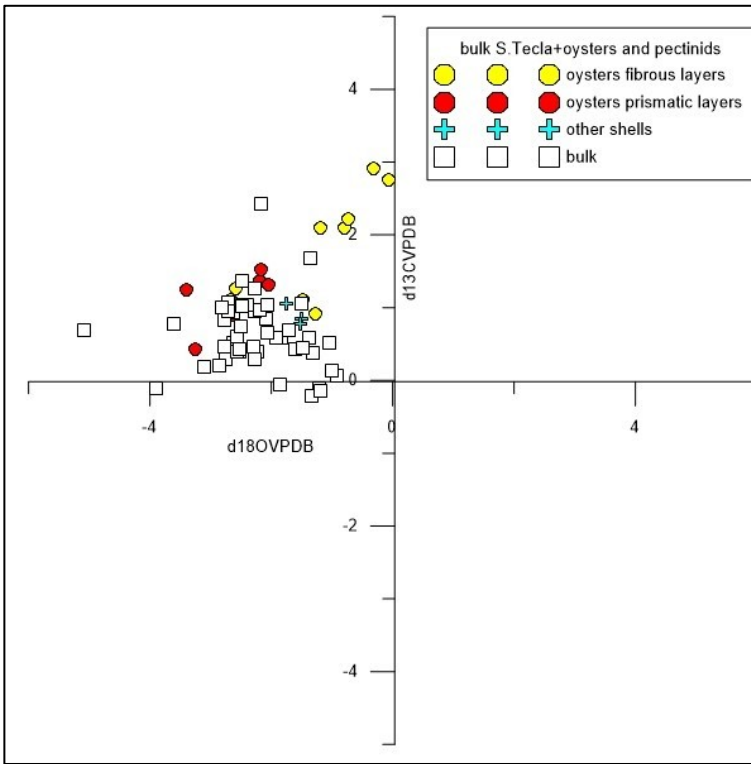


**Fig. 26:** cross plots of  $\delta^{13}\text{C}$  vs  $\delta^{18}\text{O}$  VPDB of drilled bulk samples of *S.Tecla* and *Covolo Carli* (white squares), plotted together with those of oysters (yellow dots for fibrous layers and red dots for prismatic layers) and other shells (i.e. pectinids)(light blue crosses).

As already seen at Castelgomberto, low-Mg calcite of oysters have a more pristine isotopic composition which is confirmed by their more positive values (Hasiuk et al., 2016). Isotopic bulk analysis shows values between -1 and -5‰ VPDB  $\delta^{18}\text{O}$  and between -0.5 and 2‰ VPDB  $\delta^{13}\text{C}$  (for all details see appendix Tab. 3 and Tab. 5).

The complete dataset of Santa Tecla consists of 18 oyster samples and 50 drilled bulk samples. A t-test for independent samples has been made to determine if there is a difference between the means of the two groups at a standard significance threshold of 95%. We assume a normal distribution of the values without outliers. Mean  $\delta^{13}\text{C}$  VPDB for oysters is 1.44 ‰ with standard deviation of 0.69 ‰, while the mean  $\delta^{13}\text{C}$  VPDB for bulk is 0.70‰ with standard deviation of 0.57‰. The difference between means is 0.74 ‰ which is extremely

statistically significant with  $t(66) = 4.4631$ ;  $p$ -value = 0.0001. "t(66)" stands for a t statistic with a 66 degrees of freedom (the degrees of freedom being equal to the number of samples, minus 2).

We also prepared a  $\delta^{18}\text{O}$  VPDB vs  $\delta^{13}\text{C}$  VPDB plot to compare C and O values from drilled powders and ground bulk powders (Fig. 27).

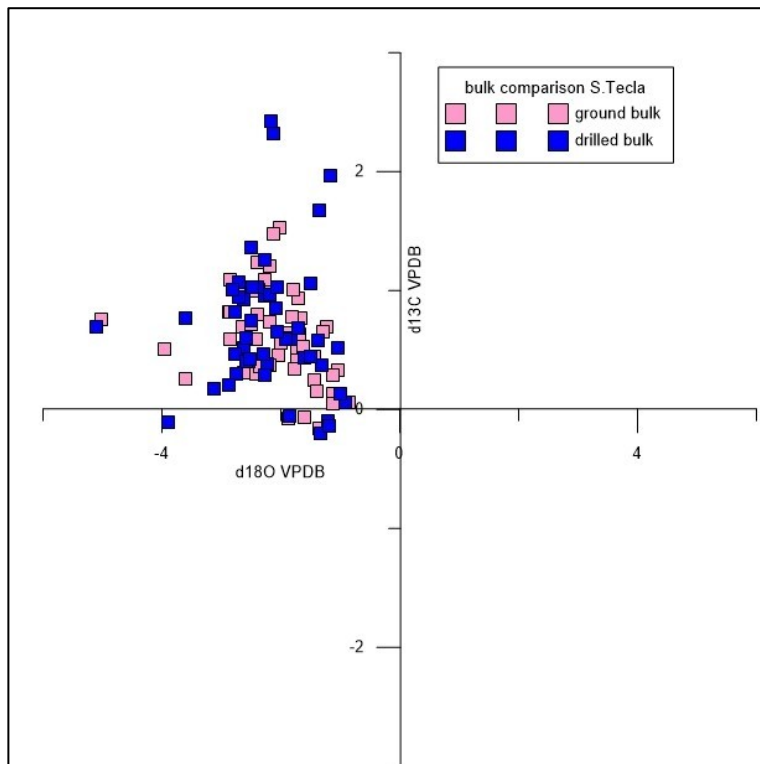


**Fig. 27: Comparison between drilled bulk (blue squares) and ground bulk (pink squares) powders from the Santa Tecla section.**

Two groups show very similar distribution (for all details see appendix Tab. 5 and Tab. 6).

A t-test for independent samples has been made to determine if there is a difference between the means of the drilled and ground bulk powder samples at a standard significance threshold of 95%. We assume a normal distribution of the values without outliers. Mean  $\delta^{13}\text{C}$  VPDB for drilled bulk is 0.7 ‰ with standard deviation of 0.57 ‰, while mean  $\delta^{13}\text{C}$  VPDB for ground bulk is 0.61 ‰ with

standard deviation of 0.39 ‰. The difference between means is 0.09 ‰ which is not statistically significant  $t(99)=0.9277$ ;  $p\text{-value}=0.3558$ . "t(99)" stands for a t statistic with a 99 degrees of freedom (the degrees of freedom being equal to the number of samples, minus 2). We thus assume that drilled bulk samples are good enough to be representative for the section.

Comparison between the two sections (Fig. 28) shows that all oyster samples lie around the same values and this, in turn, implies that the low-Mg calcite fibrous layer has a better preservation (Hasiuk et al., 2016). Pectinids shows a similar trend but in Castelgomberto some samples have been hardly affected by diagenesis (for more details see appendix Tab. 3).

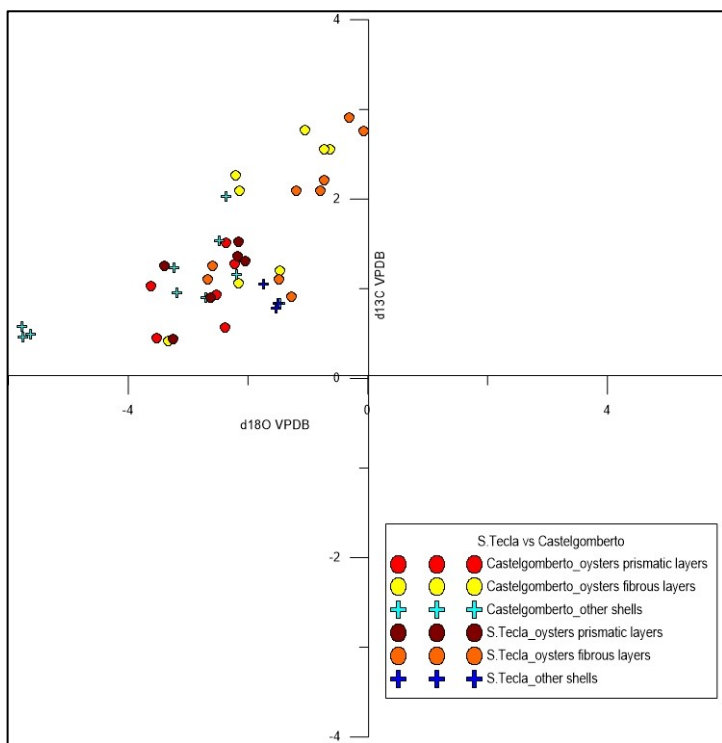


**Fig. 28: comparison between Castelgomberto (lighter colors) and Santa Tecla (darker colors). Low-Mg calcite oyster layers show more positive values than oyster prismatic layers and pectinids.**

Castelgomberto isotope values vs depth (Fig. 29) shows  $\delta^{13}\text{C}$  VPDB with values from 0.5‰ to 1.5‰ for bulk analysis but up to 3‰ for oyster fibrous layers (i.e. low-Mg calcite). On the other hand,  $\delta^{18}\text{O}$  VPDB shows negative values from -2‰ to -5‰ for bulk but close to -0.5‰ for oyster fibrous layers (for more details see appendix Tab. 3 and Tab. 4).

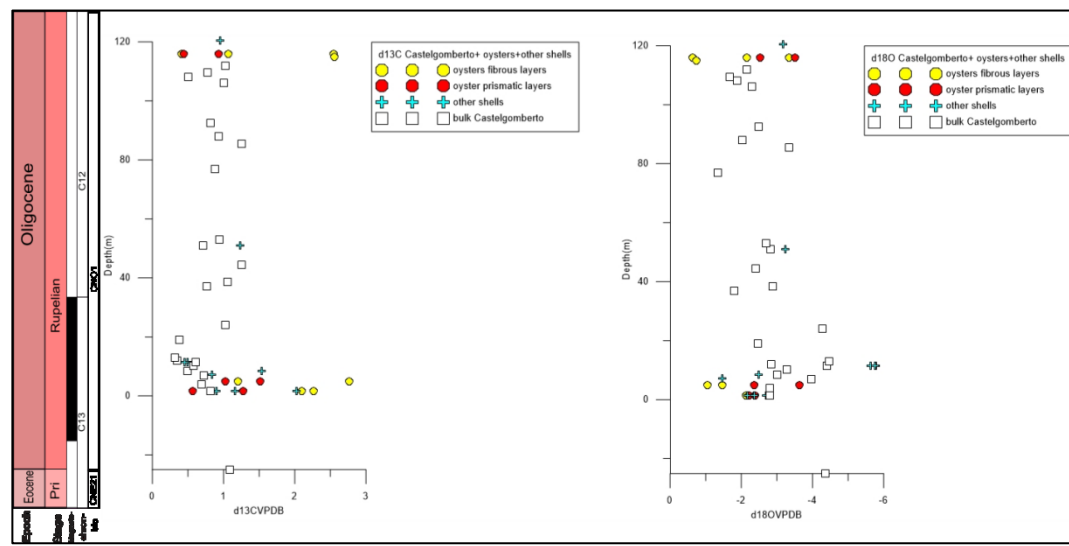


**Fig. 29:** Plot along depth of  $\delta^{13}\text{C}$  VPDB and  $\delta^{18}\text{O}$  VPDB at Castelgomberto: bulk, oysters and pectinids  $\delta^{13}\text{C}$  VPDB on the left and  $\delta^{18}\text{O}$  VPDB on the right.

Carbon and Oxygen isotope values from Santa Tecla (Fig. 30) show  $\delta^{13}\text{C}$  VPDB ranging from -0.5 ‰ to 2.5 ‰ for bulk analysis but up to 3 ‰ for oyster fibrous layers (i.e. low-Mg calcite). Carbon isotope bulk values also show more positive values at the base of the section followed by a rapid decline.  $\delta^{18}\text{O}$  VPDB values range from -1 ‰ to -4 ‰ for bulk but up to 0 ‰ for oyster fibrous layers (for more details see appendix Tab. 3 and Tab. 5).

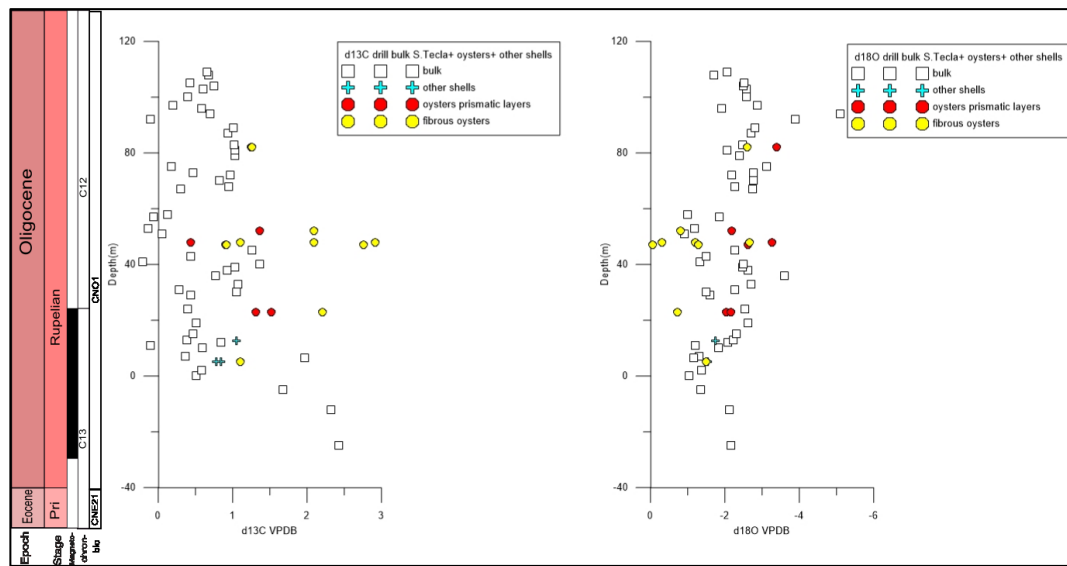


**Fig. 30:** Plot of Santa Tecla: bulk, oysters and pectinids along the depth.  $\delta^{13}\text{C}$  VPDB on the left and  $\delta^{18}\text{O}$  VPDB on the right.

### 3.4. Calcium carbonate content

From the series of MAQ1 with variable weight, a calibration straight line was calculated (Fig. 31).

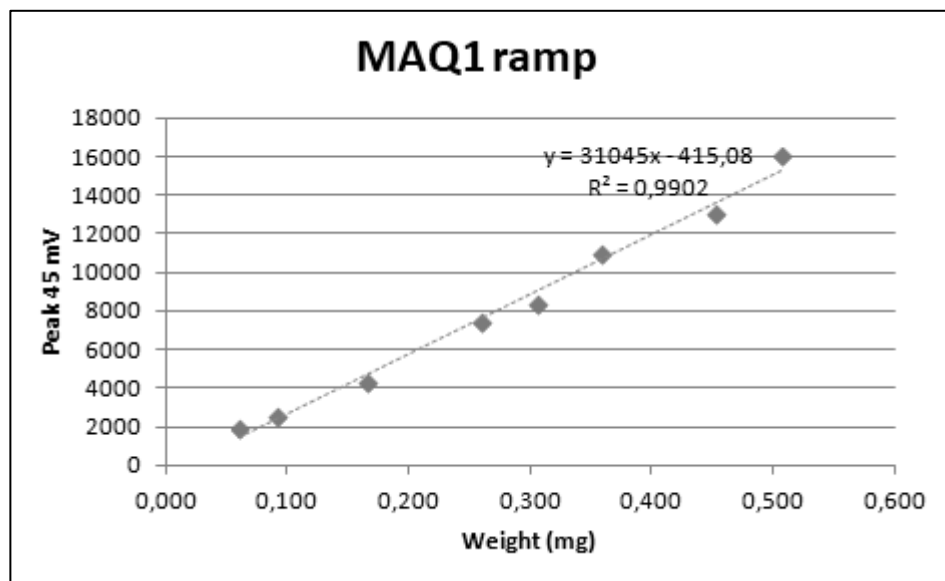


Fig. 31: plot of weight vs in the response of the mass spectrometer CCD collector set for m/z 45 (transduced into mV) of MAQ1 samples specifically prepared with increasing weight. Linear trend line with formula and  $R^2$  are shown in the plot.

With the formula  $\frac{(Peak\ mV - Intercept)}{Slope}$  the calculation of  $\text{CaCO}_3$  in mg was made for each sample and then turn in percent (for more details see appendix Tab. 7). Histogram of number of samples with percent of  $\text{CaCO}_3$  (Fig. 32) and plot of  $\text{CaCO}_3$  along depth (Fig. 33) are presented.

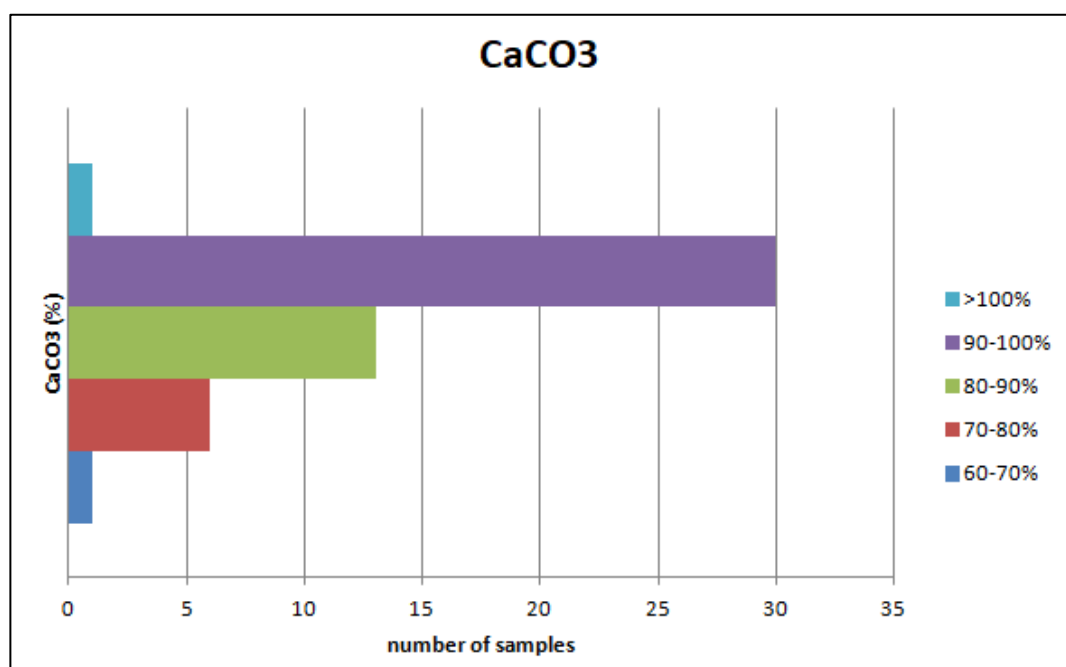


Fig. 32: Histogram plot of the number of samples for each class of CaCO<sub>3</sub> concentration.

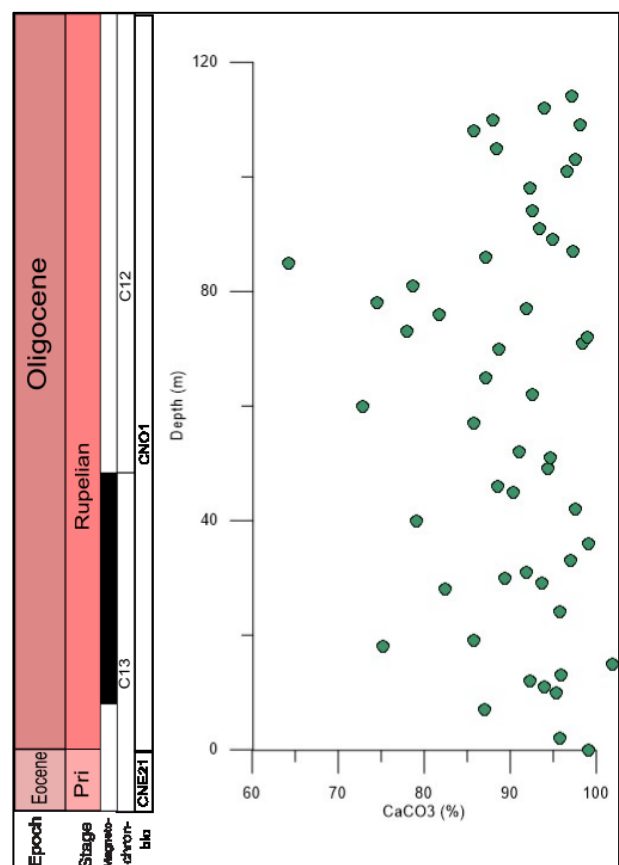


Fig. 33: Plot of CaCO<sub>3</sub> percentage (%) along the Santa Tecla section.

## 4. Discussion

### 4.1. Facies analysis

The facies observed in the field and on thin sections have been interpreted as representing parts of a distally steepened carbonate ramp, according to Pomar et al. (2017), Milizia (2019) and Preto et al. (2019):

- Facies A/B: middle/outer ramp, oligophotic zone with *maerl* facies association and rhodoliths;
- Facies C: middle ramp, meso-oligophotic zone under fair weather wave base with corals having a mesophotic ecology;
- Facies D: inner ramp, euphotic zone. Facies with encrusting foraminifera like that of Cava Valle are interpreted as derived from seagrass meadows;
- Facies E: outer ramp aphotic zone with planktonic foraminifera.

These environments are arranged in a distally steepened ramp model (Fig. 34).

It is worth noting that samples yielded calcareous nannofossils all belong to facies B and E, i.e., those facies that deposited in the deepest parts of the carbonate ramp profile.

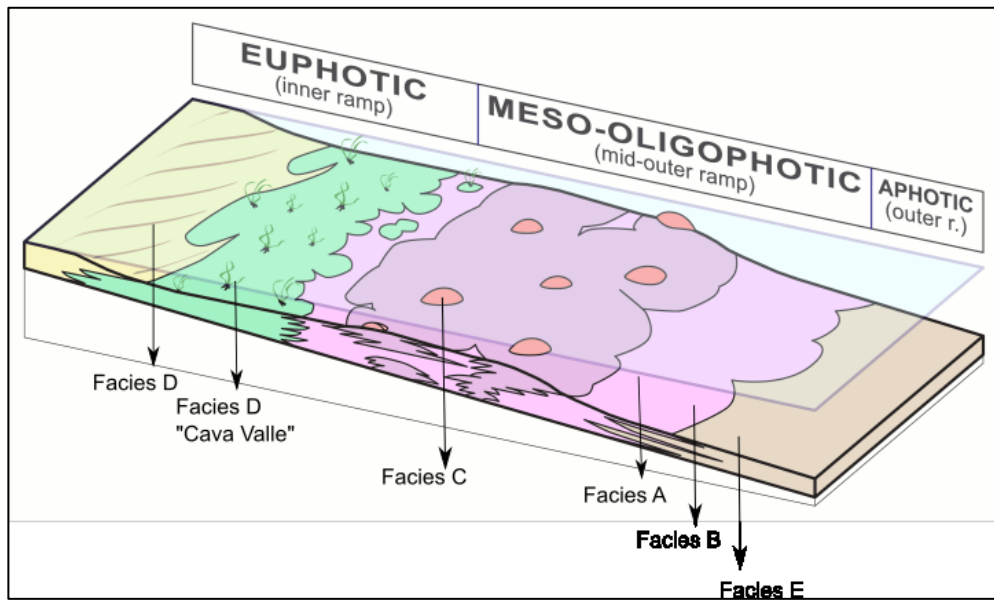


Fig. 34: distally steepened ramp model with facies association adopted for this thesis. Image from Pietra di Vicenza (Lower Oligocene, Northern Italy): proposal for designation as Global Heritage Stone Resource", Preto, N. et al. (2019)

## 4.2. Calcareous nannofossil biostratigraphy and biochronological implications

The biostratigraphic classification is based on the scheme by Agnini et al., (2014). The poor preservation and the scarcity of calcareous nannofossils made the application of any biozonal scheme difficult, especially the recognition of the acme interval of *C. subdistichus*. Specifically we have assumed that the continuous presence of this taxon can be correlated with its acme interval.

As written before, not all Castelgomberto smear slides contain nannofossil and from those only two contain index species:

- Sample FCCN21 at stratigraphic height 97.40 m, belongs to Zone CNO1 (Agnini et al., 2014). The biostratigraphic classification is based on the absence of rosette-shaped discoasters and the presence of *E.formosa*, which constrain this sample to zones CNE21-CNO1. The presence of

*C.subdistichus* further refine the biostratigraphic assignment to Zone CNO1 (Rupelian).

- Sample FCCN08 at stratigraphic height 37 m, belongs to CNO1 (Agnini et al., 2014). The biostratigraphic classification is based on the absence of rosette-shaped discoasters and the presence of *E.formosa*, which constrain this sample to zones CNE21-CNO1. The presence of *R.umbilicus* and *C.subdistichus* further refines the biostratigraphic assignment to Zone CNO1 (Rupelian).

On the other hand, the analysis on calcareous nannofossil assemblages from the S.Tecla section result in a more continuous biostratigraphic record:

- FCSTN09 at stratigraphic height 100.5 m, belongs to undifferentiated zones CNE21-CNO1 (Agnini et al., 2014). The biostratigraphic classification is based on the absence of rosette-shaped discoasters and the presence of *E.formosa*, which constrain this sample to zone CNE21-CNO1. The absence of *C.subdistichus* does not allow further refinement but the presence of *C.reticulatum* suggest an older age for this sample (zones CNE19-CNO1). This estimation is deeply biased by the presence of common reworked nannofossils, which biostratigraphic position is not consistent with the general stratigraphy of the section.
- FCSTN07b at stratigraphic height 55 m, belongs to Zone CNO1 (Agnini et al., 2014). The biostratigraphic classification is based on the absence of rosette-shaped discoasters and the presence of *E. formosa*, which constrain this sample to zones CNE21-CNO1. The presence of *R. umbilicus* and *C. subdistichus* further refines the biostratigraphic assignment to Zone CNO1 (Rupelian).
- FCSTN07a at stratigraphic height 54.5 m, belongs to Zone CNO1 (Agnini et al., 2014). The biostratigraphic classification is based on the absence of rosette-shaped discoasters and the presence of *E. formosa*, which

constrain this sample to zones CNE21-CNO1. The presence of *R. umbilicus* and *C. subdistichus* further refines the biostratigraphic assignment to Zone CNO1 (Rupelian).

- FCSTN07c at stratigraphic height 54 m, belongs to Zone CNO1 (Agnini et al., 2014). The biostratigraphic classification is based on the absence of rosette-shaped discoasters and the presence of *E. formosa*, which constrain this sample to zones CNE21-CNO1. The presence of *R. umbilicus* and *C. subdistichus* further refines the biostratigraphic assignment to Zone CNO1 (Rupelian).
- FCSTN04 at stratigraphic height 13.5 m, belongs to Zone CNO1 (Agnini et al., 2014). The biostratigraphic classification is based on the absence of rosette-shaped discoasters and the presence of *E. formosa*, which constrain this sample to zones CNE21-CNO1. The presence of *R. umbilicus* and *C. subdistichus* further refines the biostratigraphic assignment to Zone CNO1 (Rupelian).
- FCSTN02 at stratigraphic height 6.5 m, belongs to undifferentiated zones CNE21-CNO1 (Agnini et al., 2014). The biostratigraphic classification is based on the absence of rosette-shaped discoasters and the presence of *E. formosa*, which constrain this sample to zone CNE21-CNO1. The absence of *C. subdistichus* does not allow further refinement but the presence of *C. reticulatum* suggest an older age for this sample (zones CNE19-CNO1). This estimation is deeply biased by the presence of common reworked nannofossils, which biostratigraphic position is not consistent with the general stratigraphy of the section.

The study sections both belongs to Zone CNO1 (Agnini et al., 2014) or Subzone CP16b (Okada and Bukry, 1980) or Zone NP21 (Martini, 1971).

The biostratigraphic classification based on calcareous nannofossils also provides a new result. At both Castelgomberto and S.Tecla, the youngest age estimation is

still within the first biochronozone of the Early Oligocene. Since the study succession almost reaches the top of the hill where "*Arenarie e Calcaro di S.Urbano*", which have a Chattian age, starts to crop out, this is likely means that there is a gap in deposition of ~4.45 My.

Moreover, based on the estimated age of the "Pietra di Vicenza", which substantially corresponds to EOB and the biostratigraphic constrains based on calcareous nannofossils, a calculation of sedimentary rate is possible. At Castelgomberto, the section covers 158 m from the base of "Pietra di Vicenza" horizon, the youngest dating is Top of Zone CNO1 (32.92 Ma) (Agnini et al., 2014) thus the sedimentation rate for Lower Oligocene in this area is of at least 164.6 m/My. At Santa Tecla, the section covers 135 m from the base of "Pietra di Vicenza" horizon, the youngest dating obtained is Zone CNO1 (Agnini et al., 2014) thus the sedimentation rate in this area is of at least 140 m/My. These sedimentation rates are decidedly high and detailed geodynamic reconstructions as well as the subtraction of a sea-level rise occurring at the base of the Oligocene (Miller et al., 2005) are needed in order to better explain these anomalously high accumulation rates.

### 4.3. Isotopic data interpretation

As shown before, the bulk  $\delta^{18}\text{O}$  VPDB record from both Castelgomberto and Santa Tecla sections have been deeply affected by diagenesis, as testified by more negative values of the bulk samples with respect to those of calcitic bivalve shells (Hasiuk et al., 2016) (Fig. 29 and Fig. 30). The global  $\delta^{18}\text{O}$  VPDB values observed in the interval of interest varies from 0.98‰ to 1.60‰ (Westerhold et al., 2014; Pälike et al., 2006) and are substantially different from those of our dataset, thus indicating the pervasive diagenesis biasing the study samples (Fig. 35 and Fig. 36). Based on these reasons, the  $\delta^{18}\text{O}$  VPDB curve has been excluded from further interpretations.

Regarding the  $\delta^{13}\text{C}$  VPDB records, the oyster values are the most positive and in this is likely related to oyster carbon fractionation (Fig. 29 and Fig. 30). This is not unexpected, because in many faunal groups carbon disequilibrium is relatively common phenomenon related to both kinetic and vital effects (Marshall, 1992). Expected values obtained from the global  $\delta^{13}\text{C}$  VPDB vary from 0.66‰ to 0.99‰ (Westerhold et al., 2014; Pälike et al., 2006) while oysters display more positive values thus further suggesting a peculiar fractionation of this group (Fig. 35 and Fig. 36).

However, the bulk isotope analysis values overlap, and nicely fit with the global reference curve in the interval of interest suggesting that the pristine  $\delta^{13}\text{C}$  was not substantially altered (Fig. 35 and Fig. 36).

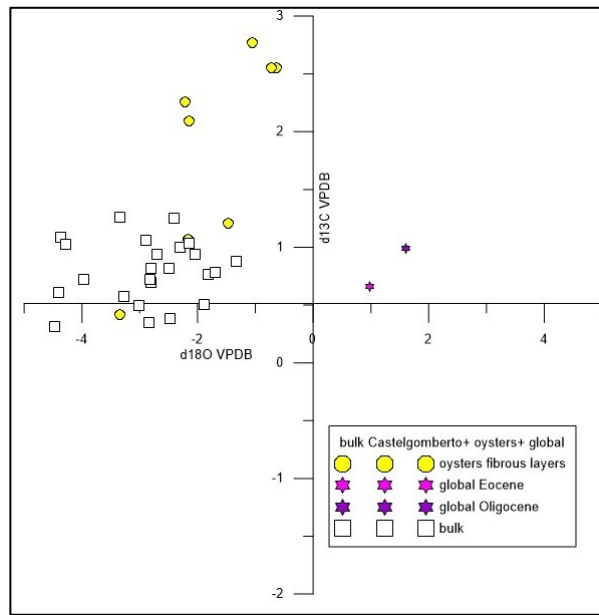


**Fig. 35:** plot of Castelgomberto bulk analysis (white squares), oysters low-Mg calcite (yellow dots), mean global values for Eocene (purple) and Oligocene (violet). Values for  $\delta^{13}\text{C}$  VPDB are close to the expected (i.e. global) but  $\delta^{18}\text{O}$  VPDB is inconsistent due to diagenesis effect.

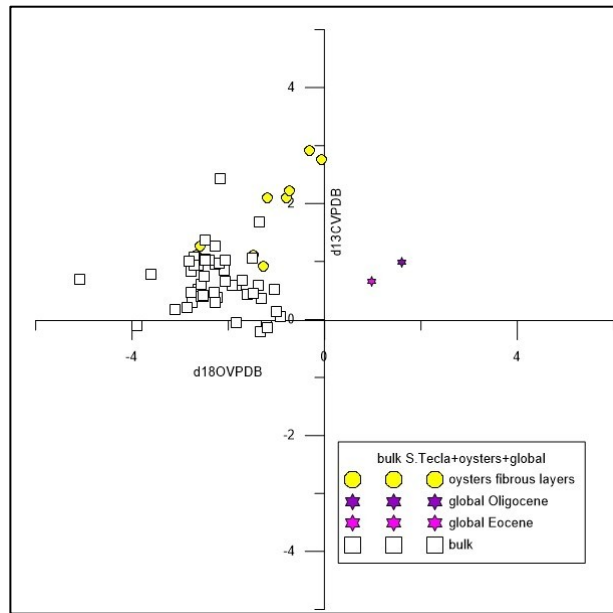


**Fig. 36:** plot of Santa Tecla drilled bulk analysis (white squares), oysters low-Mg calcite (yellow dots), mean global values for Eocene (purple) and Oligocene (violet). Values for  $\delta^{13}\text{C}$  VPDB are close to the expected (i.e. global) but  $\delta^{18}\text{O}$  VPDB is inconsistent due to diagenesis effect.

A comparison between the  $\delta^{13}\text{C}$  VPDB of the S.Tecla section and the reference curve (Westerhold et al., 2020) highlights a common trend, that is a rapid negative shift of ca.-1‰ occurring right after the EOB followed by constant interval in which the  $\delta^{13}\text{C}$  values are always close to 0‰ VPDB (Fig. 37).

In the Castelgomberto section the same trend is also present but much less apparent probably due to the lower sampling resolution in the lower part (Fig. 38). Here, in fact, only one sample was available from Cava Valle, and a short gap in the outcrop follows the basal part.

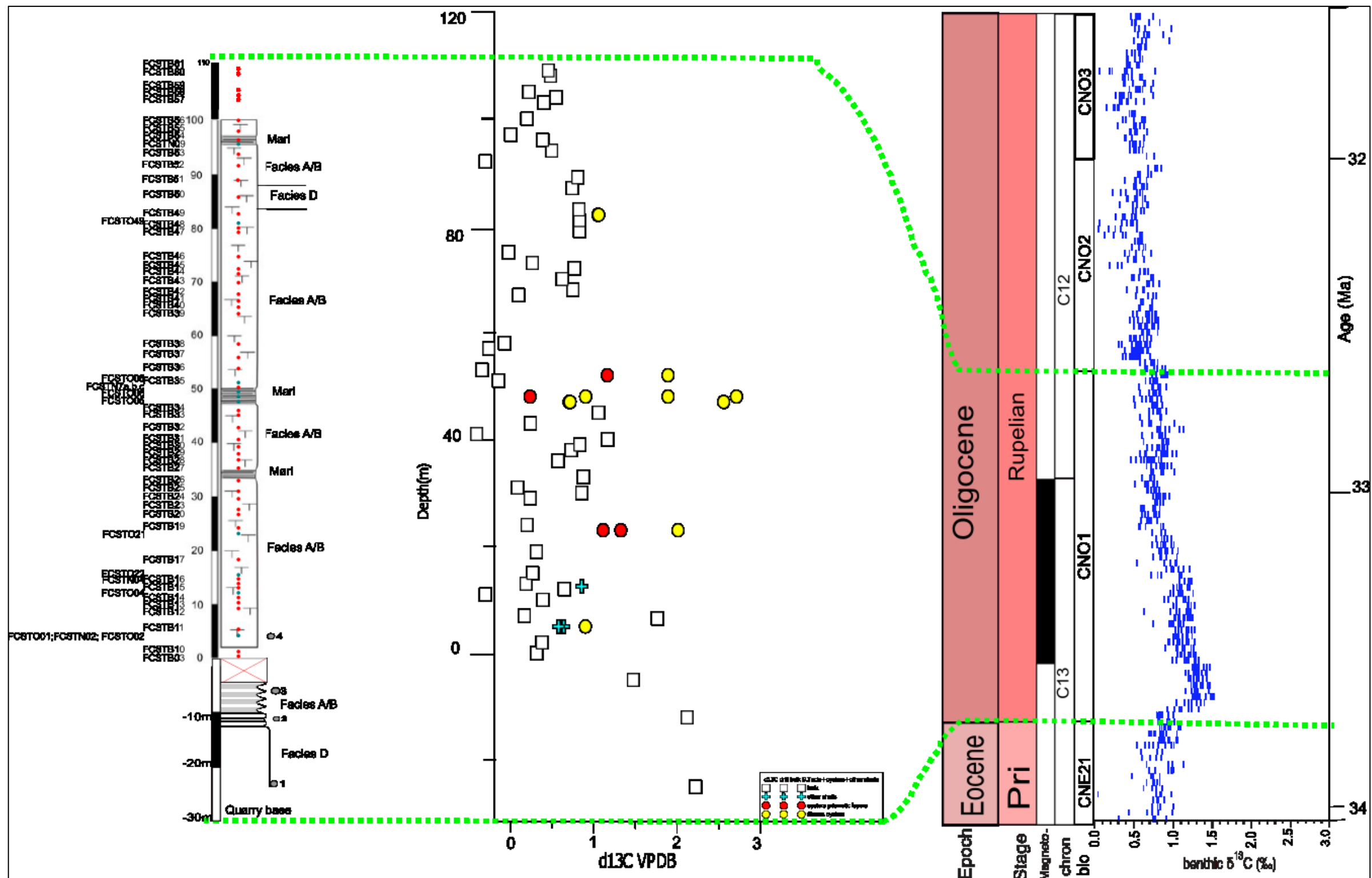


Fig. 37: composite log of Santa Tecla section with the  $\delta^{13}\text{C}$  VPDB of bulk, oysters and pectinids, correlated with (Westerhold et al., 2020) isotopic global reference curve. As highlighted by green lines, the section is constrained between the EOT at the base and by the age of 32.87 Ma at the top (top of CNO1). Note how the  $\delta^{13}\text{C}$  VPDB from analysis made the same shift as the isotopic curve presented by (Westerhold et al., 2020).

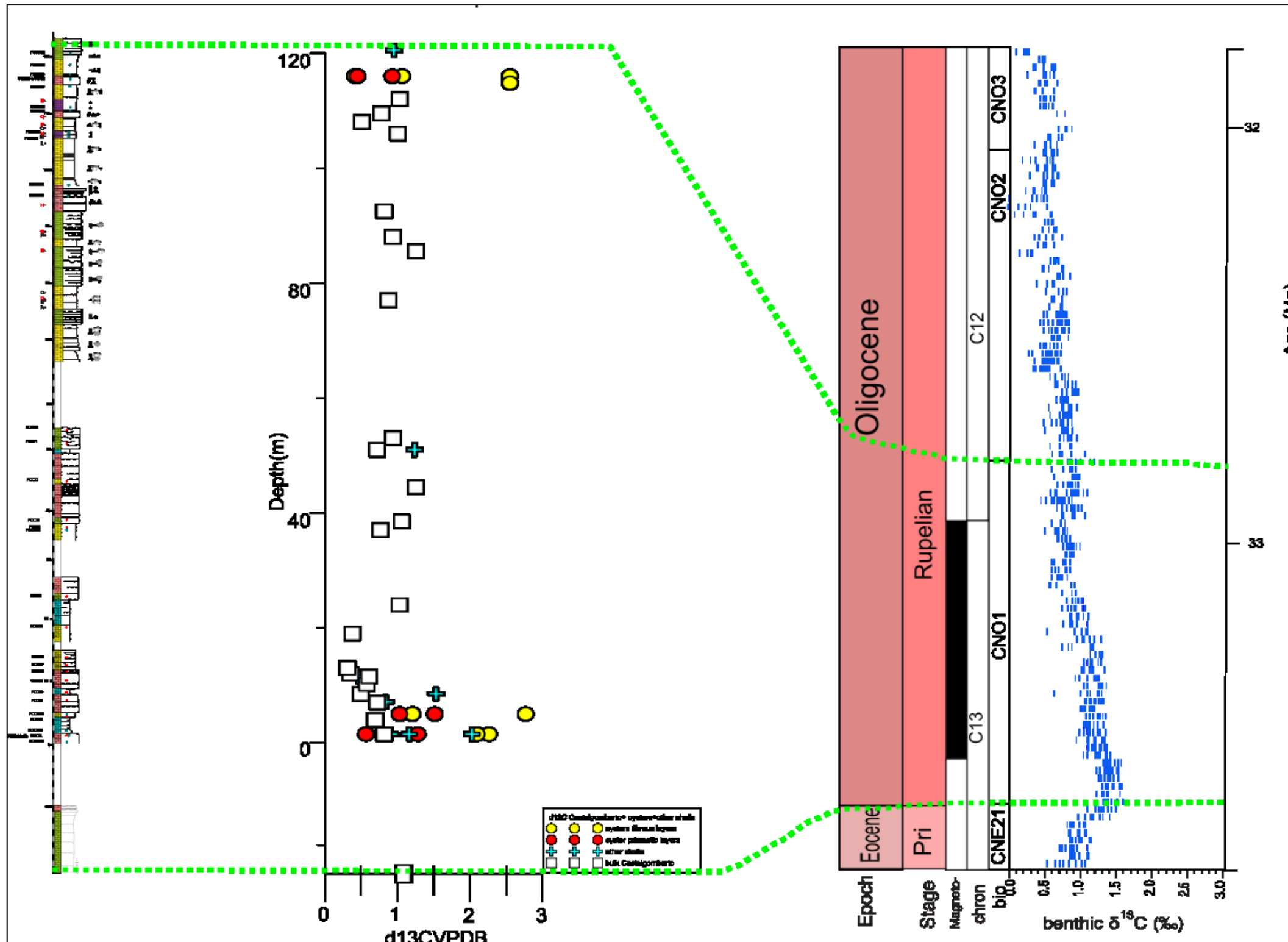


Fig. 38: composite log of Castelgomberto with the  $\delta^{13}\text{C}_{\text{VPDB}}$  of bulk, oysters and pectinids, correlated with (Westerhold et al., 2020) isotopic global reference curve. As highlighted by green lines, the section is constrained between EOT at the base and the age of 32.87 Ma at the top (top of CNO1). Note that sample from Cava Valle shows higher value which shifts closer to 0‰ for all the section. Note how the  $\delta^{13}\text{C}_{\text{VPDB}}$  from analysis made the same shift as the isotopic curve presented by (Westerhold et al., 2020).

## 5. Conclusions

$\delta^{13}\text{C}$  VPDB isotopic data collected from two section of the Castelgomberto formation, both beginning at the Eocene/Oligocene boundary, seem to nicely correlate to the global reference curve. A shift observed in the Santa Tecla section is similar to the one presented by Westerhold et al., (2020) and supported by the calcareous nannofossil biostratigraphy which ascribed the study section to Zone CNO1 (Top of Zone CNO1 is within Chron C12r)(Agnini et al., 2014). Because of the low sample spacing a degree of uncertainty still remains on the proposed interpretation. Moreover, in the Castelgomberto section this negative carbon isotope trend is present but less clear and more sampling and analysis are thus needed.

Other important results essentially based on the biostratigraphic classification are, on one side, the possible presence of ~4.45 My sedimentary gap between the Lower Oligocene Castelgomberto formation and the Upper Oligocene Arenarie di Sant'Urbano and, on the other side, the high sedimentation rates of 164 m/My and 135 m/My calculated in the Castelgomberto and the Santa Tecla sections respectively. These accumulation rates are a minimum figure, obtained assuming that the whole Zone CNO1 is present, and are unexpectedly high but they may still reconcile with the geodynamic contest of the Venetian pre-Alps, once a detailed sea level curve is being taken into account.

With this work, we introduce some starting points for future studies such as the search, in Priabonian deposits, of the negative  $\delta^{13}\text{C}$  VPDB shift that precedes the positive values found here. Finding a consistent curve will allow to precisely date Castelgomberto and Santa Tecla sections which implies a better knowledge of the lack of sedimentation experienced in the area.

In addition, if a good  $\delta^{18}\text{O}$  signal is found, a better tying of sea level curve with the local stratigraphy may be possible, along with a better understanding of geodynamic and sedimentation rates of the area.

## Acknowledgments

Acknowledgments to Department of Geosciences, University of Padua, for the availability of laboratories and Lisa Santello and Carlotta Betto that kindly helped during thesis work. I thank the professors who during these years have made my studies an unforgettable experience, and in particular my supervisor Nereo Preto and co-supervisor Claudia Agnini for the knowledge, the willingness and impeccable coordination. A special thank to all my friends that shared with me this experience and to my mother and boyfriend that always supported me.

## Bibliography

- Agnini, C., Fornaciari, E., Raffi, I., Catanzariti, R., Pälike, H., Backman, J., Rio, D., 2014. Biozonation and biochronology of Paleogene calcareous nannofossils from low and middle latitudes. *Newsletters Stratigr.* 47, 131–181.  
<https://doi.org/10.1127/0078-0421/2014/0042>
- Bassi, D., 2005. Larger foraminiferal and coralline algal facies in an Upper Eocene storm-influenced, shallow-water carbonate platform (Colli Berici, north-eastern Italy). *Palaeogeogr. Palaeoclimatol. Palaeoecol.* 226, 17–35.  
<https://doi.org/10.1016/j.palaeo.2005.05.002>
- Bassi, D., Hottinger, L., Nebelsick, J.H., 2007. Larger foraminifera from the upper Oligocene of the Venetian area, north-east Italy. *Palaeontology* 50, 845–868. <https://doi.org/10.1111/j.1475-4983.2007.00677.x>
- Brandano, M., Tomassetti, L., Cornacchia, I., 2019. The lower Rupelian cluster reefs of Majella platform, the shallow water record of Eocene to Oligocene transition. *Sediment. Geol.* 380, 21–30.  
<https://doi.org/10.1016/j.sedgeo.2018.11.013>
- Cahuzac, B., Poignant, A., 1997. An attempt of biozonation of the Oligo-Miocene in the European basins , by means of larger neritic foraminifera [ Article @ Essai de biozonation de l' Oligo-Miocène dans les bassins européens à l' aide des grands foraminifères nérithiques ]. *Bull. la Soc. Geol. Fr.* 168 (2), 155–169.
- Cherobin, D., 2015. Piattaforme carbonatiche oligoceniche nell'area vicentina: confronto tra successioni statografiche di affioramento e di sottosuolo. Università di Padova.
- Cornacchia, I., Brandano, M., Raffi, I., Tomassetti, L., Flores, I., 2018. The Eocene–Oligocene transition in the C-isotope record of the carbonate successions in the Central Mediterranean. *Glob. Planet. Change* 167, 110–122.  
<https://doi.org/10.1016/j.gloplacha.2018.05.012>

- Cornale, P., Rosanò, P., Alberti, E., Princivalle, A., 1994. Le pietre tenere del vicentino: uso e restauro. Associazione Artigiani della Provincia di Vicenza Camera di Commercio Industria Artigianato Agricoltura di Vicenza Amministrazione Provinciale di Vicenza Consorzio artigiani restauratori veneti.
- Coxall, H.K., Pearson, P., 2007. The Eocene-Oligocene Transition The Eocene – Oligocene Transition.
- De Vecchi, G., Gregnanin, A., Piccirillo, E.M., 1976. Tertiary volcanism in the veneto: Magmatology, petrogenesis and geodynamic implications. *Geol. Rundschau* 65, 701–710. <https://doi.org/10.1007/BF01808487>
- Frost, S.H., 1981. Castelgomberto 57,08. Soc. Econ. Paleontol. Mineral. SPECIAL PU, P 483 539.
- Geinster, J., Ungaro, S., 1977. The Oligocene coral formation of the Colli Berici (Vicenza, northern Italy). *Eclogae Geologicae Helvetiae* 70/3, 811–823. <https://doi.org/10.5169/seals-164644>
- Hasiuk, F.J., Kaczmarek, S.E., Fullmer, S.M., 2016. Diagenetic origins of the calcite Microcrystals that host Microporosity in limestone reservoirs. *J. Sediment. Res.* 86, 1163–1178. <https://doi.org/10.2110/jsr.2016.69>
- Houben, A.J.P., van Mourik, C.A., Montanari, A., Coccioni, R., Brinkhuis, H., 2012. The Eocene-Oligocene transition: Changes in sea level, temperature or both? *Palaeogeogr. Palaeoclimatol. Palaeoecol.* 335–336, 75–83. <https://doi.org/10.1016/j.palaeo.2011.04.008>
- Insalaco, E., 1998. The descriptive nomenclature and classification of growth fabrics in fossil scleractinian reefs. *Sediment. Geol.* 118, 159–186. [https://doi.org/10.1016/S0037-0738\(98\)00011-6](https://doi.org/10.1016/S0037-0738(98)00011-6)
- Marshall, J.D., 1992. Climatic and oceanographic isotopic signals from the carbonate rock record and their preservation. *Geol. Mag.* 129, 143–160. <https://doi.org/10.1017/S0016756800008244>
- Martini, E., 1971. Standard palaeogene calcareous nannoplankton zonation.

- Nature 226, 560–561. <https://doi.org/10.1038/226560a0>
- Mártoní, E., Zampieri, D., Kázmér, M., Dunkl, I., Frisch, W., 2011. New Paleocene-Eocene paleomagnetic results from the foreland of the Southern Alps confirm decoupling of stable Adria from the African plate. *Tectonophysics* 504, 89–99. <https://doi.org/10.1016/j.tecto.2011.03.006>
- Maruzzo, A., 2019: Proposta di istituzione del geosito “ventidotti e Covolo Carli”, Costozza, Regione Veneto. Tesi di laurea inedita, Dipartimento di Geoscienze, Università di Padova. Relatore: Preto N. The log is also available at geosite page of Veneto Region website.
- Mateu-Vicens, G., Pomar, L., Ferràndez-Cañadell, C., 2012. Nummulitic banks in the upper Lutetian “Buil level”, Ainsa basin, South Central Pyrenean Zone: the impact of internal waves. *Sedimentology*, 59, 527–552, doi: 10.1111/j.1365-3091.2011.01263.x.
- Milizia, E., 2019. AMBIENTE DEPOSIZIONALE DELLA “ PIETRA DI VICENZA ” E CRITERI PER LA DISTINZIONE. Università di Padova.
- Miller, K.G., Kominz, M.A., Browning, J. V., Wright, J.D., Mountain, G.S., Katz, M.E., Sugarman, P.J., Cramer, B.S., Christie-Blick, N., Pekar, S.F., 2005. The phanerozoic record of global sea-level change. *Science* (80-. ). 310, 1293–1298. <https://doi.org/10.1126/science.1116412>
- Nebelsick, J.H., Bassi, D., Lempp, J., 2013. Tracking paleoenvironmental changes in coralline algal-dominated carbonates of the Lower Oligocene Calcarenitì di Castelgomberto formation (Monti Berici, Italy). *Facies* 59, 133–148. <https://doi.org/10.1007/s10347-012-0349-6>
- Nebelsick, J.H., Rasser, M.W., Bassi, D., 2005. Facies dynamics in Eocene to Oligocene circumalpine carbonates. *Facies* 51, 197–217. <https://doi.org/10.1007/s10347-005-0069-2>
- Okada, H., Bukry, D., 1980. SUPPLEMENTARY MODIFICATION AND INTRODUCTION OF CODE NUMBERS TO THE LOW-LATITUDE COCCOLITH BIOSTRATIGRAPHIC ZONATION 5, 1–22.

- Pälike, H., Norris, R.D., Herrle, J.O., Wilson, P.A., Coxall, H.K., Lear, C.H., Shackleton, N.J., Tripati, A.K., Wade, B.S., 2006. The heartbeat of the Oligocene climate system. *Science* (80- ). 314, 1894–1898.  
<https://doi.org/10.1126/science.1133822>
- Pearson, P.N., Foster, G.L., Wade, B.S., 2009. Atmospheric carbon dioxide through the Eocene-Oligocene climate transition. *Nature* 461, 1110–1113.  
<https://doi.org/10.1038/nature08447>
- Pomar, L., Baceta, J.I., Hallock, P., Mateu-Vicensa, G., Bassod, D., 2017. Reef building and carbonate production modes in the west-central Tethys during the Cenozoic, *Sedimentology*. Elsevier Ltd. <https://doi.org/10.1007/s10347-005-0069-2>
- Premoli Silva, I., and D. G. Jenkins (1993), Decision on the Eocene-Oligocene boundary stratotype, *Episodes*, 16, 379– 38
- Preto N., Brandano M., Cornale P., Mazzoli C., Milizia E., Tomassetti L., 2019. Pietra di Vicenza (lower Oligocene, northern Italy): proposal for designation as Global Heritage Stone Resource. 34th IAS Meeting of Sedimentology, September 10-13, 2019, Rome, Italy.
- Spofforth, D.J.A., Agnini, C., Pälike, H., Rio, D., Fornaciari, E., Giusberti, L., Luciani, V., Lanci, L., Muttoni, G., 2010. Organic carbon burial following the middle Eocene climatic optimum in the central western Tethys. *Paleoceanography* 25, 1–11. <https://doi.org/10.1029/2009PA001738>
- Westerhold, T., Marwan, N., Drury, A.J., Liebrand, D., Agnini, C., Anagnostou, E., Barnet, J.S.K., Bohaty, S.M., De Vleeschouwer, D., Florindo, F., Frederichs, T., Hodell, D.A., Holbourn, A.E., Kroon, D., Lauretano, V., Littler, K., Lourens, L.J., Lyle, M., Pälike, H., Röhl, U., Tian, J., Wilkens, R.H., Wilson, P.A., Zachos, J.C., 2020. An astronomically dated record of Earth's climate and its predictability over the last 66 million years. *Science* (80- ). 369, 1383–1388.  
<https://doi.org/10.1126/SCIENCE.ABA6853>
- Westerhold, T., Röhl, U., Pälike, H., Wilkens, R., Wilson, P.A., Acton, G., 2014.

Orbitally tuned timescale and astronomical forcing in the middle Eocene to early Oligocene. Clim. Past 10, 955–973. <https://doi.org/10.5194/cp-10-955-2014>

## Appendix

Tab. 1: Calcareous nannofossil count results from the Castelgomberto section. The abundance of taxa is reported for each sample and each taxon.

ID sample	FCCN02	FCCN03	FCCN21	FCCN08	FCCN09
Depth (m)	118,50	117,00	97,40	37,00	2,10
<i>Biantholithus</i>					9
<i>Braarudosphaera</i>			3		
<i>Chiasmolithus solitus</i>			4	2	
<i>Clausicoccus subdistichus</i>			20	9	7
<i>Coccolithus crassus</i>				4	
<i>Coccolithus pelagicus</i>		1	522,6	78	56
<i>Cribrocentrum erbae</i>				9	
<i>Cribrocentrum isabellae</i>					
<i>Cribrocentrum reticulatum</i>			7	16	
<i>Cyclicargolithus floridanus</i>		16	2597,40	203,78	127
<i>Dictyococcites bisectus</i>					
<i>Dictyococcites</i>			48	18	19
<i>Discoaster barbadiensis</i>				1	
<i>Discoaster tanii</i>			1	1	
<i>Ericsonia formosa</i>			63	37	
<i>Fragments</i>			19	17	9
<i>Helicosphaerae</i>				1	
<i>Micula</i>				9	

<i>Prediscosphaera</i>					
<i>Reticulofenestra daviesii</i>		5			
<i>Reticulofenestra spp</i>		8	577,2	53	29
<i>Reticulofenestra umbilicus</i>				1	
<i>Sphenolithus moriformis</i>		5	475,8	34	19
<i>Sphenolithus radians</i>			3		
<i>Sphenolithus distensus</i>					
<i>Sphenolithus predistensus</i>				2	
<i>Thoracosphaerae</i>	936	74,2		19	34
<i>Toweius</i>					
<i>Watznaueria</i>				12	
Total nannofossil	0	35	4341	507,78	275
Total Field of View	468	371	390	443	465
<i>Biantholithus/mm<sup>2</sup></i>	0,00	0	0	0,00	0,97
<i>Braarudosphaera /mm<sup>2</sup></i>	0,00	0	0,38		
<i>Chiasmolithus solitus/mm<sup>2</sup></i>	0,00	0	0,51	0,23	0,00
<i>Clausicoccus subdistichus/mm<sup>2</sup></i>	0,00	0	2,56	1,02	0,75
<i>Coccolithus crassus/mm<sup>2</sup></i>	0,00	0	0	0,45	0,00
<i>Coccolithus pelagicus/mm<sup>2</sup></i>	0,00	0,13	67	8,80	6,02
<i>Cribrocentrum erbae/mm<sup>2</sup></i>	0,00	0	0	1,02	0,00
<i>Cribrocentrum isabellae/mm<sup>2</sup></i>	0,00	0	0	0,00	0,00
<i>Cribrocentrum reticulatum/mm<sup>2</sup></i>	0,00	0	0,90	1,81	0,00
<i>Cyclicargolithus floridanus/mm<sup>2</sup></i>	0,00	2,16	333	23,00	13,66
<i>Dictyococcites bisectus/mm<sup>2</sup></i>	0,00	0	0	0,00	0,00

<i>Dictyococcites/mm<sup>2</sup></i>	0,00	0	6,15	2,03	2,04
<i>Discoaster barbadiensis/mm<sup>2</sup></i>	0,00	0	0	0,11	0,00
<i>Discoaster tanii/mm<sup>2</sup></i>	0,00	0	0,13	0,11	0,00
<i>Ericsonia formosa/mm<sup>2</sup></i>	0,00	0	8,08	4,18	0,00
<i>Fragments/mm<sup>2</sup></i>	0,00	0	2,44	1,92	0,97
<i>Helicosphaerae/mm<sup>2</sup></i>	0,00	0	0	0,11	0,00
<i>Micula/mm<sup>2</sup></i>	0,00	0	0	1,02	0,00
<i>Prediscosphaera /mm<sup>2</sup></i>	0,00	0	0	0,00	0,00
<i>Reticulofenetra daviesii/mm<sup>2</sup></i>	0,00	0,67	0	0,00	0,00
<i>Reticulofenestra spp/mm<sup>2</sup></i>	0,00	1,08	74	5,98	3,12
<i>Reticulofenestra umbilicus/mm<sup>2</sup></i>	0,00	0	0	0,11	0,00
<i>Sphenolithus moriformis/mm<sup>2</sup></i>	0,00	0,67	61	3,84	2,04
<i>Sphenolithus radians/mm<sup>2</sup></i>	0,00	0	0,38	0,00	0,00
<i>Sphenolithus distensus/mm<sup>2</sup></i>	0,00	0	0	0,00	0,00
<i>Sphenolithus predistensus/mm<sup>2</sup></i>	0,00	0	0	0,23	0,00
<i>Thoracosphaerae /mm<sup>2</sup></i>	100,00	10	0	2,14	3,66
<i>Toweius/mm<sup>2</sup></i>	0,00	0	0	0,00	0,00
<i>Watznaueria/mm<sup>2</sup></i>	0,00	0	0	1,35	0,00
Total nannofossil /mm <sup>2</sup>	0,00	4,72	556,54	57,31	29,57
Total Reworked /mm <sup>2</sup>	0,00	0,00	1,92	6,21	0,97
Biozone (Agnini et all. 2014)		??	CNO1	CNO1	??

Comments	Campione sterile	no markers	Presenza di C.subdistichus, E.formosa	Presenza di C.subdistichus, E.formosa e R. umbilicus; molto rimaneggiato	no markers
Out of counting				Toweius, Dictyococcites bisectus	

Tab. 2: Calcareous nannofossil count results from the Santa Tecla section. The abundance of taxa is reported for each sample and each taxon.

ID sample	FCSTN09	FCSTN07 b	FCSTN07 a	FCSTN07 c	FCSTN04	FCSTN02
Depth (m)	100,5	55	54,5	54	13,5	6,5
<i>Biantholithus</i>	3				18	8
<i>Chiasmolithus solitus</i>				3		
<i>Clausicoccus subdistichus</i>		14	7	12	7	
<i>Coccolithus crassus</i>						
<i>Coccolithus pelagicus</i>	18	28	25	27	203	35
<i>Cribrocentrum erbae</i>						

<i>Cribrocentrum isabellae</i>						
<i>Cribrocentrum reticulatum</i>	5	4			6	
<i>Cyclicargolithus floridanus</i>	368,1	151	56	99	406	152
<i>Dictyococcites bisectus</i>	5	2			1	3
<i>Dictyococcites</i>	14	29	8	15	44	14
<i>Discoaster barbadiensis</i>						
<i>Discoaster tanii</i>					2	
<i>Ericsonia formosa</i>	12	3	9		26	11
<i>Fragments</i>	19	12	7	15		8
<i>Helicosphaerae</i>						
<i>Prediscosphaera</i>						1
<i>Reticulofenestra spp</i>	18	52	50	51	44	
<i>Reticulofenestra umbilicus</i>						
<i>Sphenolithus moriformis</i>	39	27	25	36	51	13
<i>Sphenolithus radians</i>	1		1			
<i>Sphenolithus distensus</i>						
<i>Sphenolithus anarrhopus</i>		2		3		
<i>Thoracosphaerae</i>	98,16		56	48	73,08	23
<i>Retecapsa</i>			1			
<i>Watznaueria</i>						
Total nannofossil	502,1	324	189	261	808	244
Totale Fields of View	409	520	463	507	406	448
<i>Biantholithus/m m<sup>2</sup></i>	0,37	0	0,00	0,00	2,22	0,89
<i>Chiasmolithus solitus/mm<sup>2</sup></i>	0,00	0	0,00	0,30	0,00	0,00

<i>Clausicoccus subdistichus/mm<sup>2</sup></i>	0,00	1,35	0,76	1,18	0,86	0,00
<i>Coccolithus crassus/mm<sup>2</sup></i>	0,00	0	0,00	0,00	0,00	0,00
<i>Coccolithus pelagicus/mm<sup>2</sup></i>	2,20	2,69	2,70	2,66	25,00	3,91
<i>Cribrocentrum erbae/mm<sup>2</sup></i>	0,00	0	0,00	0,00	0,00	0,00
<i>Cribrocentrum isabellae/mm<sup>2</sup></i>	0,00	0	0,00	0,00	0,00	0,00
<i>Cribrocentrum reticulatum/mm<sup>2</sup></i>	0,61	0,38	0,00	0,00	0,74	0,00
<i>Cyclicargolithus floridanus/mm<sup>2</sup></i>	45,00	14,52	6,05	9,76	50,00	16,96
<i>Dictyococcites bisectus/mm<sup>2</sup></i>	0,61	0,19	0,00	0,00	0,12	0,33
<i>Dictyococcites/m m<sup>2</sup></i>	1,71	2,79	0,86	1,48	5,42	1,56
<i>Discoaster barbadiensis/mm<sup>2</sup></i>	0,00	0	0,00	0,00	0,00	0,00
<i>Discoaster tani/mm<sup>2</sup></i>	0,00	0	0,00	0,00	0,25	0,00
<i>Ericsonia formosa/mm<sup>2</sup></i>	1,47	0,29	0,97	0,00	3,20	1,23
<i>Fragments/mm<sup>2</sup></i>	2,32	1,15	0,76	1,48	0,00	0,89
<i>Helicosphaerae/m m<sup>2</sup></i>	0,00	0	0,00	0,00	0,00	0,00
<i>Prediscosphaera/ mm<sup>2</sup></i>	0,00	0	0,00	0,00	0,00	0,11
<i>Reticulofenestra spp/mm<sup>2</sup></i>	2,20	5	5,40	5,03	5,42	0,00
<i>Reticulofenestra umbilicus/mm<sup>2</sup></i>	0,00	0	0,00	0,00	0,00	0,00

<i>Sphenolithus moriformis/mm<sup>2</sup></i>	4,77	2,60	2,70	3,55	6,28	1,45
<i>Sphenolithus radians/mm<sup>2</sup></i>	0,12	0	0,11	0,00	0,00	0,00
<i>Sphenolithus distensus/mm<sup>2</sup></i>	0,00	0	0,00	0,00	0,00	0,00
<i>Sphenolithus anarrhopus/mm<sup>2</sup></i>	0,00	0,19	0,00	0,30	0,00	0,00
<i>Thoracosphaerae /mm<sup>2</sup></i>	12,00	0	6,05	4,73	9,00	2,57
<i>Retecaps/mm<sup>2</sup></i>	0,00	0	0,11	0,00	0,00	0,00
<i>Watznaueria/mm<sup>2</sup></i>	0,00	0	0,00	0,00	0,00	0,00
Total nannofossil /mm <sup>2</sup>	61,38	31,15	20,41	25,74	99,51	27,23
Total Reworked /mm <sup>2</sup>	0,98	0,58	0,11	0,59	3,20	0,89
Biozone (Agnini et all. 2014)	CNE21	CNO01	CNO01	CNO01	CNO01	CNE21
Comments	Presenza di D.bisectus e E.formosa, no Discoaster e no C.subdistichus	Presenza di C.subdistichus, E.formosa	Presenza di C.subdistichus, E.formosa	Presenza di C.subdistichus	Presenza di C.subdistichus, E.formosa	Presenza di D.bisectus e E.formosa, no Discoaster e no C.subdistichus

Tab. 3:  $\delta^{13}\text{C}$  VPDB and  $\delta^{18}\text{O}$  VPDB of oysters and pectinids from Castelgomberto and S.Tecla

Analysis	sample	weight	Peak 45	d13C	d18O	<b>d13C vpdb</b>	<b>d18O vpdb</b>	depth (m)
54125	FCC01a	0,248	7242	44,03	41,07	<b>1,16</b>	<b>-2,18</b>	1,5
54134	FCC01b	0,365	10147	43,76	40,53	<b>0,90</b>	<b>-2,70</b>	1,5
54138	FCC11b	0,285	6508	45,17	41,05	<b>2,26</b>	<b>-2,21</b>	1,5
54149	FCCO11a	0,328	9377	44,93	40,89	<b>2,03</b>	<b>-2,36</b>	1,5
54144	FCCO11b	0,282	8291	43,40	40,86	<b>0,56</b>	<b>-2,39</b>	1,5
54141	FCCO11bF1	0,352	10133	45,00	41,12	<b>2,10</b>	<b>-2,14</b>	1,5
54151	FCCO11bP2	0,286	8694	44,15	41,03	<b>1,28</b>	<b>-2,22</b>	1,5
54146	FCCO10	0,438	13121	43,89	39,57	<b>1,03</b>	<b>-3,63</b>	5
54139	FCCO10F1	0,243	7536	44,07	41,82	<b>1,21</b>	<b>-1,47</b>	5
54136	FCCO10F2	0,231	6896	45,70	42,25	<b>2,77</b>	<b>-1,06</b>	5
54148	FCCO10P2	0,331	10033	44,39	40,88	<b>1,51</b>	<b>-2,37</b>	5
54128	FCC03	0,315	7101	43,69	41,82	<b>0,84</b>	<b>-1,47</b>	7,1
54127	FCC04	0,361	8626	44,41	40,76	<b>1,53</b>	<b>-2,48</b>	8,5
54140	FCC06a	0,459	12231	43,41	37,32	<b>0,58</b>	<b>-5,78</b>	11,5
54135	FCC06b	0,233	5720	43,33	37,47	<b>0,50</b>	<b>-5,63</b>	11,5
54147	FCC06C	0,373	11005	43,29	37,35	<b>0,46</b>	<b>-5,76</b>	11,5
54142	FCC14	0,455	12584	44,10	39,97	<b>1,24</b>	<b>-3,24</b>	51
54133	FCCO07F1	0,248	7485	45,48	42,59	<b>2,55</b>	<b>-0,73</b>	114,8
54130	FCCO04F1	0,307	8855	43,92	41,10	<b>1,06</b>	<b>-2,16</b>	116
54124	FCCO04P1	0,322	9441	43,78	40,71	<b>0,93</b>	<b>-2,53</b>	116
54131	FCCO05	0,353	10572	45,47	42,69	<b>2,55</b>	<b>-0,64</b>	116
54126	FCCO06F1	0,227	7266	43,25	39,87	<b>0,41</b>	<b>-3,34</b>	116
54143	FCCO06P1	0,347	10221	43,28	39,68	<b>0,45</b>	<b>-3,52</b>	116
54150	FCCO01	0,358	10552	43,80	40,03	<b>0,95</b>	<b>-3,19</b>	120,5
54162	FCSTO01	0,333	6162	43,96	41,80	<b>1,10</b>	<b>-1,49</b>	5
54155	FCSTO02a	0,266	6253	43,69	41,79	<b>0,84</b>	<b>-1,50</b>	5
54152	FCSTO02b	0,324	6485	43,63	41,76	<b>0,78</b>	<b>-1,53</b>	5
54157	FCSTO04	0,326	9626	43,91	41,53	<b>1,05</b>	<b>-1,75</b>	12,5
54163	FCSTO05F1	0,234	4396	45,69	43,28	<b>2,76</b>	<b>-0,07</b>	47
54165	FCSTO05F2	0,262	5139	43,77	42,02	<b>0,92</b>	<b>-1,28</b>	47
54171	FCSTO05P1	0,311	8951	43,76	40,62	<b>0,90</b>	<b>-2,62</b>	47
54160	FCSTO06F1	0,27	7464	45,00	42,10	<b>2,09</b>	<b>-1,20</b>	48
54170	FCSTO06F2	0,205	5272	43,96	40,56	<b>1,10</b>	<b>-2,67</b>	48
54173	FCSTO06F3	0,221	6421	45,85	43,02	<b>2,91</b>	<b>-0,32</b>	48
54168	FCSTO06P1	0,318	9385	43,27	39,95	<b>0,43</b>	<b>-3,26</b>	48
54154	FCSTO08F1	0,287	8089	44,99	42,52	<b>2,09</b>	<b>-0,80</b>	52
54159	FCSTO08P1	0,213	5757	44,24	41,08	<b>1,36</b>	<b>-2,18</b>	52
54156	FCSTO21F1	0,242	6553	45,12	42,59	<b>2,21</b>	<b>-0,73</b>	23
54158	FCSTO21P1	0,236	2469	44,18	41,22	<b>1,31</b>	<b>-2,04</b>	23
54167	FCSTO21P2	0,343	9479	44,40	41,10	<b>1,53</b>	<b>-2,16</b>	23
54172	FCSTO49F1	0,284	8702	44,13	40,65	<b>1,26</b>	<b>-2,59</b>	82
54166	FCSTO49P1	0,375	10110	44,12	39,81	<b>1,25</b>	<b>-3,39</b>	82

54123	Gr 1	0,451	13174	43,57	32,69	0,72	-10,22	
54132	Gr 1	0,442	13062	43,57	32,63	0,73	-10,28	
54164	Gr 1	0,221	6736	43,47	32,91	0,63	-10,01	
54174	Gr 1	0,277	8267	43,46	32,81	0,62	-10,10	
54121	Maq 1	0,211	6265	45,56	42,22			
54122	Maq 1	0,537	16089	45,60	42,19			
54129	Maq 1	0,296	8973	45,53	42,13			
54137	Maq 1	0,446	13260	45,57	42,13			
54145	Maq 1	0,372	11192	45,52	42,15			
54153	Maq 1	0,315	9331	45,49	42,13			
54161	Maq 1	0,221	6372	45,42	42,15			
54169	Maq 1	0,285	8581	45,44	42,14			
54175	Maq 1	0,277	8361	45,45	42,18			
54176	Maq 1	0,372	11194	45,47	42,11			

Tab. 4:  $\delta^{13}\text{C}$  VPDB and  $\delta^{18}\text{O}$  VPDB of bulk from Castelgomberto

Analysis	sample	weight	Peak 45	d13C	d18O	d13C vpdb	d18O vpdb	Depth (m)
55833	04-ACV1	0.303	9048	43,92	38,85	<b>1,09</b>	<b>-4,37</b>	-25,00
55823	FCC01	0.298	8476	43,64	40,49	<b>0,82</b>	<b>-2,80</b>	1,50
55822	FCC02	0.296	8202	43,51	40,48	<b>0,69</b>	<b>-2,81</b>	4,00
55841	FCC03	0.323	9621	43,54	39,28	<b>0,72</b>	<b>-3,96</b>	7,00
55851	FCC04	0.312	8915	43,31	40,27	<b>0,50</b>	<b>-3,01</b>	8,50
55830	FCC05	0.206	6212	43,39	39,99	<b>0,58</b>	<b>-3,28</b>	10,20
55843	FCC06	0.262	7705	43,43	38,82	<b>0,61</b>	<b>-4,40</b>	11,50
55840	FCC07	0.295	8359	43,16	40,44	<b>0,35</b>	<b>-2,85</b>	12,00
55836	FCC08	0.195	5429	43,12	38,74	<b>0,31</b>	<b>-4,47</b>	13,00
55825	FCC09	0.206	5069	43,19	40,83	<b>0,38</b>	<b>-2,47</b>	19,00
55824	FCC10	0.364	10969	43,86	38,94	<b>1,03</b>	<b>-4,29</b>	24,00
55846	FCC11	0.322	7500	43,59	41,52	<b>0,76</b>	<b>-1,81</b>	37,00
55832	FCC12	0.335	9296	43,89	40,40	<b>1,06</b>	<b>-2,89</b>	38,50
55827	FCC13	0.313	7420	44,10	40,91	<b>1,25</b>	<b>-2,40</b>	44,50
55839	FCC14	0.298	6400	43,54	40,47	<b>0,72</b>	<b>-2,81</b>	51,00
55837	FCC15	0.213	5696	43,77	40,59	<b>0,94</b>	<b>-2,70</b>	53,00
55852	C	0.284	6556	43,70	42,02	<b>0,88</b>	<b>-1,33</b>	77,00
55853	E	0.318	9150	44,10	39,92	<b>1,26</b>	<b>-3,34</b>	85,50
55845	G	0.242	7146	43,76	41,28	<b>0,93</b>	<b>-2,04</b>	88,00
55849	H	0.301	8308	43,64	40,81	<b>0,82</b>	<b>-2,49</b>	92,50
55829	N	0.189	4188	43,84	41,01	<b>1,00</b>	<b>-2,30</b>	106,00
55848	P	0.266	6983	43,32	41,44	<b>0,51</b>	<b>-1,89</b>	108,00
55821	Q	0.246	6862	43,60	41,65	<b>0,78</b>	<b>-1,69</b>	109,50
55835	R	0.259	4256	43,86	41,17	<b>1,03</b>	<b>-2,15</b>	112,00

55820	GR1	0.308	8782	43,48	32,65	0,67	-10,31	
55844	GR1	0.248	7289	43,48	32,76	0,66	-10,21	
55854	GR1	0.251	4137	43,38	32,74	0,57	-10,23	
55818	MAQ1	0.202	5669	45,53	42,26			
55819	MAQ1	0.369	10683	45,52	42,23			
55826	MAQ1	0.303	8885	45,54	42,19			
55834	MAQ1	0.290	6604	45,52	42,15			
55842	MAQ1	0.274	8173	45,50	42,17			
55850	MAQ1	0.270	8083	45,42	42,17			
55855	MAQ1	0.280	8558	45,41	42,21			
55856	MAQ1	0.317	9570	45,41	42,29			

Tab. 5:  $\delta^{13}\text{C}$  VPDB and  $\delta^{18}\text{O}$  VPDB of drilled bulk from S.Tecla

Analysis	sample	weight	Peak 45	d13C	d18O	<b>d13C vpdb</b>	<b>d18O vpdb</b>	Depth (m)
55357	FCSTB03	0,227	4323	43,27	42,38	<b>0,51</b>	<b>-1,04</b>	0
55346	FCSTB10	0,345	9748	43,34	42,03	<b>0,58</b>	<b>-1,38</b>	2
55355	FCSTB11	0,247	5781	43,12	42,09	<b>0,37</b>	<b>-1,31</b>	7
55333	FCSTB12	0,329	6614	43,35	41,55	<b>0,59</b>	<b>-1,83</b>	10
55363	FCSTB13	0,217	4442	42,63	42,20	<b>-0,10</b>	<b>-1,21</b>	11
55329	FCSTB14	0,315	8351	43,62	41,30	<b>0,85</b>	<b>-2,07</b>	12
55327	FCSTB15	0,396	10954	43,14	41,14	<b>0,39</b>	<b>-2,22</b>	13
55319	FCSTB16	0,307	6910	43,22	41,06	<b>0,47</b>	<b>-2,30</b>	15
55334	FCSTB18	0,248	6586	43,27	40,72	<b>0,51</b>	<b>-2,63</b>	19
55339	FCSTB19	0,304	6848	43,15	40,82	<b>0,40</b>	<b>-2,53</b>	24
55315	FCSTB23	0,281	6170	43,19	41,78	<b>0,44</b>	<b>-1,61</b>	29
55330	FCSTB24	0,309	2722	43,83	41,90	<b>1,06</b>	<b>-1,50</b>	30
55317	FCSTB25	0,219	5581	43,03	41,09	<b>0,29</b>	<b>-2,27</b>	31
55351	FCSTB26	0,371	9996	43,85	40,64	<b>1,07</b>	<b>-2,71</b>	33
55322	FCSTB27	0,282	6312	43,54	39,70	<b>0,77</b>	<b>-3,60</b>	36
55337	FCSTB28	0,293	6278	43,70	40,72	<b>0,93</b>	<b>-2,63</b>	38
55353	FCSTB29	0,301	7515	43,81	40,88	<b>1,03</b>	<b>-2,47</b>	39
55343	FCSTB30	0,328	8634	44,16	40,87	<b>1,37</b>	<b>-2,49</b>	40
55321	FCSTB31	0,308	7458	42,52	42,08	<b>-0,21</b>	<b>-1,32</b>	41
55359	FCSTB32	0,24	4911	43,19	41,91	<b>0,44</b>	<b>-1,49</b>	43
55345	FCSTB33	0,335	8526	44,04	41,10	<b>1,26</b>	<b>-2,26</b>	45
55350	FCSTB35	0,281	5379	42,79	42,51	<b>0,06</b>	<b>-0,91</b>	51
55340	FCSTB36	0,304	6594	42,59	42,23	<b>-0,14</b>	<b>-1,19</b>	53
55324	FCSTB37	0,213	5582	42,67	41,54	<b>-0,06</b>	<b>-1,84</b>	57
55354	FCSTB38	0,316	7336	42,87	42,42	<b>0,13</b>	<b>-1,00</b>	58
55349	FCSTB41	0,275	7139	43,04	40,60	<b>0,30</b>	<b>-2,74</b>	67
55331	FCSTB42	0,311	8590	43,72	41,09	<b>0,95</b>	<b>-2,28</b>	68

55364	FCSTB43	0,364	9826	43,59	40,58	<b>0,82</b>	<b>-2,76</b>	70
55367	FCSTB44	0,267	6485	43,74	41,18	<b>0,97</b>	<b>-2,18</b>	72
55362	FCSTB45	0,269	6725	43,22	40,58	<b>0,46</b>	<b>-2,76</b>	73
55335	FCSTB46	0,252	6048	42,92	40,21	<b>0,18</b>	<b>-3,11</b>	75
55347	FCSTB47	0,273	7146	43,81	40,96	<b>1,03</b>	<b>-2,40</b>	79
55361	FCSTB48	0,215	5224	43,81	41,31	<b>1,03</b>	<b>-2,06</b>	81
55323	FCSTB49	0,221	6124	43,80	40,87	<b>1,02</b>	<b>-2,48</b>	83
55365	FCSTB50	0,305	7353	43,71	40,63	<b>0,94</b>	<b>-2,71</b>	87
55318	FCSTB51	0,241	6402	43,78	40,53	<b>1,01</b>	<b>-2,81</b>	89
55316	FCSTB52	0,313	8790	42,63	39,40	<b>-0,10</b>	<b>-3,90</b>	92
55342	FCSTB53	0,31	8715	43,46	38,15	<b>0,70</b>	<b>-5,09</b>	94
55325	FCSTB54	0,278	6622	43,35	41,47	<b>0,59</b>	<b>-1,91</b>	96
55356	FCSTB55	0,229	5542	42,94	40,47	<b>0,20</b>	<b>-2,86</b>	97
55326	FCSTB56	0,31	8377	43,15	40,78	<b>0,40</b>	<b>-2,57</b>	100
55366	FCSTB57	0,232	6396	43,36	40,78	<b>0,60</b>	<b>-2,57</b>	103
55348	FCSTB58	0,248	6995	43,51	40,86	<b>0,75</b>	<b>-2,49</b>	104
55358	FCSTB59	0,227	5315	43,17	40,83	<b>0,42</b>	<b>-2,52</b>	105
55332	FCSTB60	0,302	8038	43,44	41,67	<b>0,68</b>	<b>-1,71</b>	108
55341	FCSTB61	0,32	7559	43,42	41,31	<b>0,65</b>	<b>-2,06</b>	109
55831	CC1	0,301	8806	45,32	41,15	2,42	-2,16	-25,00
55828	CC2	0,299	9302	45,21	41,20	2,32	-2,12	-12,00
55838	CC3	0,227	5761	44,54	42,00	1,67	-1,35	-5,00
55847	CC4	0,337	7602	44,84	42,20	1,96	-1,16	6,50
55314	GR1	0,207	4918	43,48	32,79	0,72	-10,23	
55338	GR1	0,356	9782	43,47	32,71	0,71	-10,30	
55312	MAQ1	0,3	9453	45,48	42,27			
55313	MAQ1	0,234	7073	45,46	42,29			
55320	MAQ1	0,196	5624	45,49	42,24			
55328	MAQ1	0,237	6792	45,46	42,21			
55336	MAQ1	0,27	8153	45,45	42,20			
55344	MAQ1	0,293	8960	45,42	42,23			
55352	MAQ1	0,228	6260	45,38	42,31			
55360	MAQ1	0,255	7292	45,33	42,32			
55368	MAQ1	0,282	8118	45,33	42,30			

Tab. 6:  $\delta^{13}\text{C}$  VPDB and  $\delta^{18}\text{O}$  VPDB of ground bulk from S.Tecla

Analysis	sample	weight	Peak 45	d13C	d18O	d13C vpdb	d18O vpdb	Depth (m)
55680	FCSTB 03	0,369	11246	43,43	42,18	<b>0,69</b>	<b>-1,22</b>	0
55721	FCSTB 10	0,323	9558	43,39	42,10	<b>0,65</b>	<b>-1,29</b>	2
55686	FCSTB 11	0,348	9364	43,05	42,37	<b>0,33</b>	<b>-1,03</b>	7

55718	FCSTB 12	0,363	10666	43,17	41,65	<b>0,44</b>	<b>-1,72</b>	10
55694	FCSTB 13	0,342	9922	42,85	42,27	<b>0,14</b>	<b>-1,13</b>	11
55701	FCSTB 14	0,324	9247	43,52	41,71	<b>0,77</b>	<b>-1,67</b>	12
55714	FCSTB 15	0,306	9082	43,07	41,61	<b>0,34</b>	<b>-1,77</b>	13
55720	FCSTB 16	0,229	7289	43,18	41,32	<b>0,45</b>	<b>-2,04</b>	15
55705	FCSTB 17	0,216	5164	42,64	41,78	<b>-0,07</b>	<b>-1,60</b>	18
55672	FCSTB 18	0,234	6310	43,48	41,18	<b>0,74</b>	<b>-2,18</b>	19
55728	FCSTB 19	0,332	9825	43,10	41,18	<b>0,37</b>	<b>-2,18</b>	24
55692	FCSTB 20	0,228	5932	42,98	41,95	<b>0,25</b>	<b>-1,44</b>	28
55697	FCSTB 23	0,206	6080	43,18	41,94	<b>0,45</b>	<b>-1,44</b>	29
55681	FCSTB 24	0,228	6404	43,68	41,66	<b>0,93</b>	<b>-1,72</b>	30
55706	FCSTB 25	0,302	8613	43,38	41,52	<b>0,64</b>	<b>-1,85</b>	31
55668	FCSTB 26	0,233	7073	43,97	41,18	<b>1,20</b>	<b>-2,18</b>	33
55729	FCSTB 27	0,280	8609	43,57	40,46	<b>0,82</b>	<b>-2,86</b>	36
55709	FCSTB 28	0,243	6053	43,55	40,95	<b>0,80</b>	<b>-2,39</b>	38
55698	FCSTB 29	0,233	7110	43,77	41,08	<b>1,01</b>	<b>-2,27</b>	39
55678	FCSTB 30	0,219	6228	44,30	41,34	<b>1,53</b>	<b>-2,02</b>	40
55669	FCSTB 31	0,288	7939	42,55	42,05	<b>-0,16</b>	<b>-1,34</b>	41
55724	FCSTB 32	0,289	8463	43,26	41,64	<b>0,52</b>	<b>-1,73</b>	43
55666	FCSTB 33	0,312	9141	44,25	41,23	<b>1,47</b>	<b>-2,12</b>	45
55685	FCSTB 34	0,311	8777	42,87	41,99	<b>0,15</b>	<b>-1,40</b>	46
55682	FCSTB 35	0,230	6206	42,77	42,55	<b>0,06</b>	<b>-0,86</b>	51
55664	FCSTB 36	0,232	5356	42,76	42,27	<b>0,04</b>	<b>-1,13</b>	53
55727	FCSTB 37	0,274	7900	42,64	41,49	<b>-0,07</b>	<b>-1,88</b>	57
55673	FCSTB 38	0,214	5884	43,01	42,27	<b>0,29</b>	<b>-1,13</b>	58
55670	FCSTB 39	0,350	9596	43,52	41,56	<b>0,78</b>	<b>-1,81</b>	63
55716	FCSTB 40	0,373	11284	43,37	41,69	<b>0,63</b>	<b>-1,69</b>	64
55710	FCSTB 41	0,230	7113	43,03	40,94	<b>0,30</b>	<b>-2,41</b>	67
55689	FCSTB 42	0,335	8123	43,57	40,47	<b>0,82</b>	<b>-2,85</b>	68
55662	FCSTB 43	0,311	7905	43,85	40,48	<b>1,09</b>	<b>-2,85</b>	70
55665	FCSTB 44	0,280	8004	44,01	40,96	<b>1,24</b>	<b>-2,39</b>	72
55722	FCSTB 45	0,272	6364	43,33	40,48	<b>0,59</b>	<b>-2,85</b>	73
55717	FCSTB 46	0,226	5629	43,24	39,32	<b>0,50</b>	<b>-3,96</b>	75
55700	FCSTB 47	0,221	4553	43,86	41,08	<b>1,10</b>	<b>-2,28</b>	79
55702	FCSTB 48	0,291	7893	43,76	41,59	<b>1,00</b>	<b>-1,78</b>	81
55712	FCSTB 49	0,330	9910	43,77	40,98	<b>1,01</b>	<b>-2,37</b>	83
55704	FCSTB 50	0,285	8397	43,75	40,63	<b>0,99</b>	<b>-2,70</b>	87
55684	FCSTB 51	0,187	5527	43,75	40,87	<b>1,00</b>	<b>-2,48</b>	89
55725	FCSTB 52	0,193	5648	42,98	39,69	<b>0,26</b>	<b>-3,60</b>	92
55676	FCSTB 53	0,202	5884	43,51	38,22	<b>0,76</b>	<b>-5,02</b>	94
55708	FCSTB 54	0,367	10913	43,27	41,76	<b>0,53</b>	<b>-1,62</b>	96
55696	FCSTB 55	0,349	10495	43,04	40,72	<b>0,31</b>	<b>-2,61</b>	97
55713	FCSTB 56	0,307	8428	43,09	40,99	<b>0,36</b>	<b>-2,36</b>	100
55690	FCSTB 57	0,253	6802	43,44	40,69	<b>0,69</b>	<b>-2,64</b>	103
55677	FCSTB 58	0,329	9964	43,46	40,84	<b>0,71</b>	<b>-2,51</b>	104
55674	FCSTB 59	0,215	5962	43,33	40,94	<b>0,59</b>	<b>-2,41</b>	105
55726	FCSTB 60	0,302	8793	43,34	41,50	<b>0,60</b>	<b>-1,87</b>	108
55688	FCSTB 61	0,207	6318	43,30	41,36	<b>0,56</b>	<b>-2,00</b>	109

55661	Gr 1	0,257	7627	43,48	32,71	0,74	-10,30	
55693	Gr 1	0,210	5667	43,33	32,87	0,59	-10,14	
55731	Gr 1	0,343	9611	43,42	32,77	0,68	-10,24	
55659	Maq 1	0,253	7098	45,53	42,22			
55660	Maq 1	0,187	5094	45,58	42,22			
55667	Maq 1	0,285	8651	45,51	42,18			
55675	Maq 1	0,284	5847	45,45	42,27			
55683	Maq 1	0,328	8814	45,39	42,30			
55691	Maq 1	0,180	5393	45,34	42,29			
55699	Maq 1	0,211	5835	45,30	42,37			
55707	Maq 1	0,329	9890	45,28	42,39			
55715	Maq 1	0,248	7512	45,29	42,32			
55723	Maq 1	0,274	8720	45,33	42,21			
55732	Maq 1	0,256	8291	45,42	42,13			
55733	Maq 1	0,260	8006	45,42	42,10			
55663	Maq ramp	0,060	1955	45,66	42,22			
55671	Maq ramp	0,091	2538	45,55	42,20			
55679	Maq ramp	0,165	4365	45,42	42,29			
55687	Maq ramp	0,305	8359	45,37	42,30			
55695	Maq ramp	0,358	10990	45,33	42,40			
55703	Maq ramp	0,409	10426	45,27	42,40			
55711	Maq ramp	0,451	13112	45,31	42,35			
55719	Maq ramp	0,506	16041	45,37	42,32			

Tab. 7: CaCO<sub>3</sub> mg and CaCO<sub>3</sub> percentage from S.Tecla

Analysis	sample	weight	Peak 45	Depth (m)	CaCO3 (mg)	CaCO3%
55680	FCSTB 03	0,369	11246	0	0,36558584	<b>99,07</b>
55721	FCSTB 10	0,323	9558	2	0,30919894	<b>95,73</b>
55686	FCSTB 11	0,348	9364	7	0,30271888	<b>86,99</b>
55718	FCSTB 12	0,363	10666	10	0,3462236	<b>95,38</b>
55694	FCSTB 13	0,342	9922	11	0,32137224	<b>93,97</b>
55701	FCSTB 14	0,324	9247	12	0,29882936	<b>92,23</b>
55714	FCSTB 15	0,306	9082	13	0,29331426	<b>95,85</b>
55720	FCSTB 16	0,229	7289	15	0,23340526	<b>101,92</b>
55705	FCSTB 17	0,216	5164	18	0,16242895	<b>75,20</b>
55672	FCSTB 18	0,234	6310	19	0,20070434	<b>85,77</b>
55728	FCSTB 19	0,332	9825	24	0,31812108	<b>95,82</b>
55692	FCSTB 20	0,228	5932	28	0,18810423	<b>82,50</b>
55697	FCSTB 23	0,206	6080	29	0,19303293	<b>93,71</b>
55681	FCSTB 24	0,228	6404	30	0,2038553	<b>89,41</b>
55706	FCSTB 25	0,302	8613	31	0,27762628	<b>91,93</b>
55668	FCSTB 26	0,233	7073	33	0,22620891	<b>97,09</b>

55729	FCSTB 27	0,280	8609	36	0,27751865	<b>99,11</b>
55709	FCSTB 28	0,243	6053	40	0,19211623	<b>79,06</b>
55698	FCSTB 29	0,233	7110	42	0,22742995	<b>97,61</b>
55678	FCSTB 30	0,219	6228	45	0,19798391	<b>90,40</b>
55669	FCSTB 31	0,288	7939	46	0,25512793	<b>88,59</b>
55724	FCSTB 32	0,289	8463	49	0,27262706	<b>94,33</b>
55666	FCSTB 33	0,312	9141	51	0,29526273	<b>94,64</b>
55685	FCSTB 34	0,311	8777	52	0,28310427	<b>91,03</b>
55682	FCSTB 35	0,230	6206	57	0,19725648	<b>85,76</b>
55664	FCSTB 36	0,232	5356	60	0,16886447	<b>72,79</b>
55727	FCSTB 37	0,274	7900	62	0,25383266	<b>92,64</b>
55673	FCSTB 38	0,214	5884	65	0,18649349	<b>87,15</b>
55670	FCSTB 39	0,350	9596	70	0,31048678	<b>88,71</b>
55716	FCSTB 40	0,373	11284	71	0,36684771	<b>98,35</b>
55710	FCSTB 41	0,230	7113	72	0,22752644	<b>98,92</b>
55689	FCSTB 42	0,335	8123	73	0,26127397	<b>77,99</b>
55662	FCSTB 43	0,311	7905	76	0,25400338	<b>81,67</b>
55665	FCSTB 44	0,280	8004	77	0,25730651	<b>91,90</b>
55722	FCSTB 45	0,272	6364	78	0,20251178	<b>74,45</b>
55717	FCSTB 46	0,226	5629	81	0,17796476	<b>78,75</b>
55700	FCSTB 47	0,221	4553	85	0,1420201	<b>64,26</b>
55702	FCSTB 48	0,291	7893	86	0,25360256	<b>87,15</b>
55712	FCSTB 49	0,330	9910	87	0,32097513	<b>97,27</b>
55704	FCSTB 50	0,285	8397	89	0,27042993	<b>94,89</b>
55684	FCSTB 51	0,187	5527	91	0,17456514	<b>93,35</b>
55725	FCSTB 52	0,193	5648	94	0,17859569	<b>92,54</b>
55676	FCSTB 53	0,202	5884	98	0,18648978	<b>92,32</b>
55708	FCSTB 54	0,367	10913	101	0,35448141	<b>96,59</b>
55696	FCSTB 55	0,349	10495	103	0,34050438	<b>97,57</b>
55713	FCSTB 56	0,307	8428	105	0,27146911	<b>88,43</b>
55690	FCSTB 57	0,253	6802	108	0,21715686	<b>85,83</b>
55677	FCSTB 58	0,329	9964	109	0,32277143	<b>98,11</b>
55674	FCSTB 59	0,215	5962	110	0,18909517	<b>87,95</b>
55726	FCSTB 60	0,302	8793	112	0,2836684	<b>93,93</b>
55688	FCSTB 61	0,207	6318	114	0,20097899	<b>97,09</b>